INFLUENCE OF GEOMETRIC PARAMETERS ON 3D PERIODIC LATTICE EFFECTIVE PROPERTIES

BY

GANESH PATIL

THESIS

Submitted in partial fulfillment of the requirements
for the degree of Master of Science in Mechanical Engineering
in the Graduate College of the
University of Illinois at Urbana-Champaign, 2019

Urbana, Illinois

Adviser:

Assistant Professor Kathryn H. Matlack

Abstract

Lattice materials are generated by tessellating a unit cell, composed of a specific truss configurations, in an infinite periodicity to combine the effect of bulk material properties and geometric periodicity. They offer enhanced mechanical and dynamic properties per unit mass, and the ability to engineer the material response by optimizing the unit cell. Characterizing lattice properties through experiments can be a time consuming and costly process, so analytical and numerical methods are crucial. Specifically, the Bloch-wave homogenization approach allows one to characterize the effective static properties of the lattice unit cell while simultaneously analyzing wave propagation properties. While this analysis has been used for some time, a thorough study of this approach on 3D lattice materials with different symmetries and geometries is presented here. Using Bloch-wave homogenization, multiple periodic lattices with cubic, transversely isotropic, and tetragonal symmetry, including an auxetic geometry, over a wide range of relative densities are analyzed within a finite element framework. The effect of geometric parameters on lattice properties is discussed and a comparison between lattices based on their anisotropy index is presented. Method studied in this thesis can be extended for designing multifunctional metamaterials with optimized static and dynamic properties simultaneously. This work can also serve as the basis for nondestructive evaluation of metamaterials properties using ultrasonic velocity measurements.

This thesis is dedicated to my mother, Pushpa Patil. Her support, encouragement and constant love have sustained me throughout my life.

Acknowledgments

I would like to take this opportunity to thank a lot of people who helped me get this thesis to completion. First, I would like to thank my advisor Prof. Kathryn Matlack for her unwavering support, patience and continuous motivation throughout my program. I am also grateful to the professors for teaching some excellent courses at the university. A special mention to Prof. Petros Sofronis, Prof. Martin Ostoja-Starzewski and Prof. John Lambros for teaching courses that were directly related to my research.

It has been great pleasure to be a part of the Wave propagation and Metamaterials laboratory. I would also like to thank Ignacio Arretche, Changgong Kim, Connor Pierce and Itay Grienberg for all the technical discussions we used to have. A special mention to my labmate and roommate Chaitanya Nimmagadda for helping me at every step for last couple of years. I would also like to thank Aditya Shedge, who worked with me on the extension of this project and has shown great dedication. Finally, I thank my family for their love and encouragement throughout.

Table of Contents

List of Figures

1 Introduction

1.1 Lattice Materials

The word 'lattice' indicates the spatial repetition of a specific configuration. This specific configuration is often refers to as a representative volume element (RVE)) [1,2] or unit cell, which when repeated in space forms an infinite array of structure. Lattice materials are alternatively refered as 'phononic crystals' or 'architectured materials'. These names are derived from their counterpart - photonic crystals from electromagnetics. In general, architectured materials spans over a wide range of length scale but the lattice materials are usually of $10^{-2}m$ order. As discussed, lattice materials contain spatial repetitions of a unit cell comprised of trusses connected in a specific geometry or configuration, one such example is shown in Fig. 1. The overall dimension of the lattice unit cell is termed as 'Lattice Constant'. Two dimensional (2-D) lattice materials are tessellated along two directions within a plane while the 3rd dimension is assumed to have continuous material. On the other hand, three dimensional (3-D) lattice materials are repeated in three directions as shown in Fig. 1. These lattice materials possess better mechanical properties per unit mass compared to their parent bulk material [3, 4] and the geometric periodicity of these structures often regulates their static, dynamic, and wave propagation properties [5]. This unique feature of lattice materials opens up new areas in material property charts [6, 7] that has potential lightweight structural applications.

Lattice materials are classified based on their deformation pattern under uni-axial loading. The scaling relation between elastic modulus and relative density of the lattice materials determines whether the lattice is stretch-

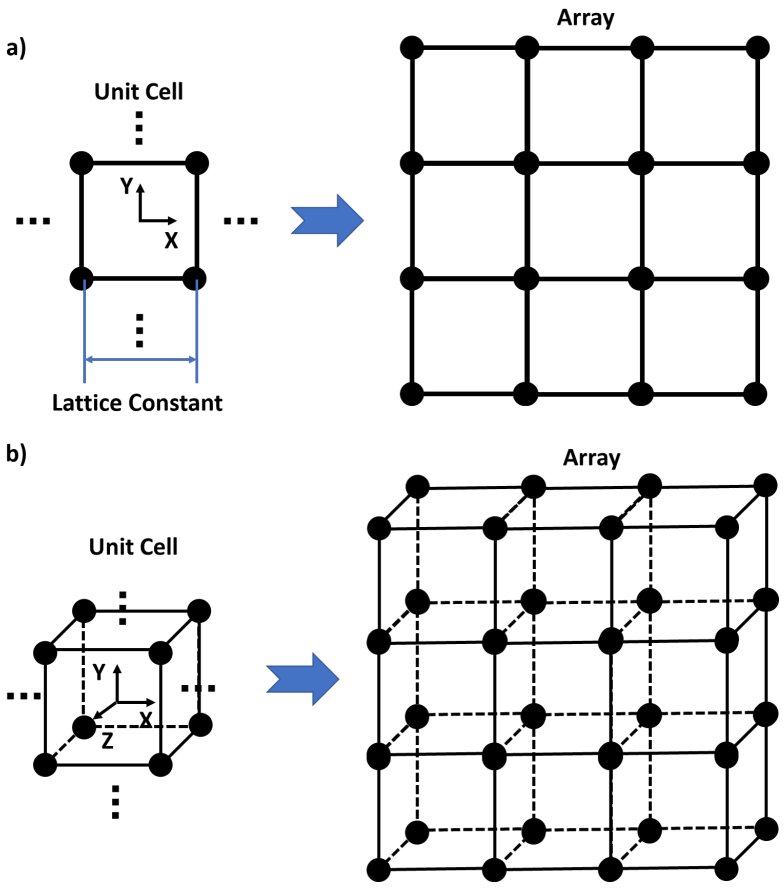

Figure 1: Schematics of (a) Two-dimensional square lattice unit cell and tessellation within plane, (b) three-dimensional cubic lattice unit cell and tessellation along three principal axis. Trusses are represented as bars and junction locations are shown through solid circles.

ing dominated or bending dominated [8]. In stretching dominated lattice, the elastic stiffness varies linearly with relative density whereas in bending dominated lattices, the elastic stiffness varies non-linearly. This non-lieanr scaling follows a power law relationship with an exponent of 2 for relative density. Bending-dominated lattices are less stiff and stronger than stretching-dominated lattices for the same relative density [9]. One can do such differentiation between lattices based on Maxwell's rule. According to this rule, a freely-supported pin-jointed lattice with number of bars, b, and number of frictionless joints, j, is statically and kinematically determinate if

$b = 2j - 3$ for 2D lattices and $b = 3j - 6$ for 3D lattices [10, 11].

1.2 Lattice Properties and Applications

Beyond static and dynamic properties, lattice materials exhibits unique properties such as negative Poisson's ratio [12, 13], negative or zero thermal coefficient of expansion [14], negligible shear stiffness [15, 16], negative mass and density [17, 18]. Along with high strength-to-weight ratio, the periodicity of lattice materials supports bragg scattering phenomenon at the unit cell interfaces. This has been exploited to create bandgaps, frequencies that do not transfer vibrations, that has potential applications as structural vibration mitigation components [5, 19–21]. Lattices with low or negative coefficient of thermal expansions are useful in thermo-mechanical applications [14, 22]. By incorporating two or more such properties within a structure, lattice materials can serve as multifunctional material in structures [23, 24]. Lattices also exhibits enhanced energy absorption (impact mitigation ability) [21, 25, 26], that can help us design blast-tolerant structures. Lattice materials can also be used as implants [27] and biomaterials [28, 29] due to their ability to generate low stresses inside cells. Some lattice materials behaves like a fluid as they have negligible shear modulus; such lattices can steer waves and can be used as cloak to make objects invisible against propagating waves [30]. Recent development on smart structures have introduced adaptive metamaterials fundamnetally based on lattice unit cells that adapt to surrounding environment [31, 32]. Overall, lattice materials are useful in wide engineering applications across various length scales from aerospace and automotive component to transportation and earthquake engineering.

1.3 Motivation

As discussed, the lattice geometry and truss configuration determines the lattice effective properties. The performance of lattice materials strongly depends on their effective properties, thus evaluating these properties is essential but at the same time not quite straightforward, specifically when the structure includes complexity in the form of symmetry and geometry. The existing methods (discussed later in section 2) are either limited to simple planar geometries or requires significant finite element calculations. Further, for these lattice materials to be adopted in structural components and applications, methods of nondestructively evaluating their properties and degradation over operation is critical. Thus relating lattice wave velocities with their effective material properties is essential. In this thesis, the Bloch-wave homogenization method for effective stiffness tensor evaluation of 3D periodic lattices with different geometries, anisotropies, and densities is outlined in detail. The lattice design parameters and relative densities are parameterized and dependence of effective property on these variables is studied. A comparison between various lattices based on their anisotropy index is presented and a way to tune the overall anisotropy of the structure is introduced.

1.4 Thesis Outline

The thesis is organized in ten sections. The organization of this thesis is as follows: Section 2 summarizes the previous work on effective property evaluation. This section highlights the overall approach being used for property evaluation and their limitations. Section 3 covers the fundamental engineering principles in the field of solid mechanics and elastic wave prop-

agation. These concepts will be helpful while studying lattice materials that possess crystal symmetries and anisotropy by virtue of their geometry. Section 4 briefly explains the different lattices under consideration. The parametric studies and independent design variables are highlighted in this section. Sections 5 and 6 review the elastostatic and Bloch-wave homogenization theories, respectively, and their corresponding FE simulation setups. Theoretical concepts behind these methods are discussed first followed by the finite element setup in commercial software. Section 7 presents results of the prototypical cubically symmetric lattices as test cases to validate the methods. Cubic symmetric lattices are compared in this section and their individual deformation behavior is discussed. Section 8 presents results of effective stiffness tensors of the tetragonally symmetric and transversely isotropic test lattices. These lattices are compared to each other based on their universal anisotropy index. An unusual wave propagation is observed in auxetic lattice and mechanics behind that wave behavior is discussed. In section 9, evaluated effective stiffness tensors of composite structures using the Bloch-wave homogenization method are presented. The thesis ends in section 10 with a set of conclusions and suggestions for future work. An article is published in the Journal of Acoustical Society of America (JASA) based on the work presented in this thesis. The article citations are https://doi.org/10.1121/1.5091690.

2 Literature Review

As discussed in previous section, evaluating lattice effective properties is essential to study different lattice configurations and its dependence on geometric parameters. There have been many efforts in past years to develop methodologies to evaluate lattice effective properties. Various numerical, computational and experimental methods have been introduced. Each have their own advantages and limitations. Some of the major contributions are discussed in this section.

In the early developments, the effective mechanical properties of 2D honeycomb and foam structures have been evaluated analytically by Gibson and Ashby [3] and of a 3D octet lattice by Deshpande et al. [33]. They developed closed form expressions for the effective mechanical properties of lattice structures. In initial analytical evaluations, lattice trusses were modeled as slender bars to study axial deformation, or as Euler-Bernoulli and Timoshenko beams to study bending deformation [3,33]. These assumptions limit the application of the theory to small relative densities. In their work, they applied uniform force to the unit cell boundaries and solved the static problem using equilibrium equations. The deformation pattern is obtained by evaluating moments and forces on each truss of the lattice unit cell. The deformations are later used to evalute the strains and thereby effective properties. Later work by Chen [34] incorporated bending as well as twisting deformation of 2D honeycomb cells using the generalized variational principle to accurately model flexural rigidity. To study the effects of height of the 2D honeycomb, Hohe and Becker [35] used a strain energy based analytical method to evaluate the stiffness tensor. Even though there has been a significant improvement in analytical methods for lattice effective property

evaluation, their use remains limited as it becomes difficult to apply them on complex 3D geometries over a wide range of densities.

To overcome the limitations and narrow feasibility band of analytical methods, finite element (FE) modeling has been explored. Scarpa et al. [36] considered 2D auxetic honeycomb structure with negative in-plane Poisson's ratio. They evaluated uniaxial Young's modulus and Poisson's ratio through static FE by considering 2-node beam elements for each truss. Wallach and Gibson [37] also used the static FE approach to evaluate the moduli of 3D structures of various aspect ratios, by modeling them as spring and truss elements while incorporating periodic boundary conditions. They considered an orthotropic lattice with 9 independent constants that needed 6 independent simulations for the stiffness tensor evaluation. This same process has been extended by Dalaq et al. [2], to evaluate the effective properties of triply periodic minimal surfaces (TPMS) but without beam modeling. The limitation with the use of static FE simulation is its demand for the higher number of simulations for anisotropic structures.

Wave propagation methods can simultaneously extract static effective properties and wave propagation properties of a material, condensing the computation time. Elsayed and Pasini [38, 39] used the Bloch-wave method in conjunction with the Cauchy-Born hypothesis (collectively called as 'Bloch-wave homogenization' hereafer) to obtain the stiffness of 2D lattices with a pin and rigid jointed architectures. Phani et al. [5] also used the Bloch-wave homogenization method for 2D isotropic lattices such as triangular, hexagonal and kagome, by modeling the trusses as Timoshenko beams. Their work was extended to anisotropic topologies by Chopra [40] and Lie et al. [41] but was restricted to planar structures. Krodel et al. [42] applied this same method to a 3D anisotropic auxetic lattice using 1D Timoshenko beam ele-

ments connected by rigid joints. Even though the wave propagation method has been around for some time, its use for effective property evaluation has not yet been fully applied and studied, specifically for 3D lattices. Modeling 3D lattices in an FE framework with 3D truss elements and without rigid joint assumptions is of prime importance in order to simulate more realistic deformations of lattice materials. For the efficient use of this approach in the design process, the wave propagation method needs to be validated on different geometries having higher anisotropy. There also exists few other methods for evaluation of effective properties such as asymptotic homogenization [9] (specifically for heterogeneous structures), homogenization based on the equation of motion [9] and dynamic equivalent continuum model [43] (incorporating microinertial effect of low density lattices) that has their own advantages and limitations but are beyond the discussion of this thesis. Further, researchers working in the field of nondestructive evaluation have explored wave propagation in anisotropic materials to predict quality (or condition) of the material through experimentally evaluated wave velocities [44–46]. However, applying this method to instead obtain the material properties of 3D periodic lattice metamaterials from wave velocities has not yet been fully explored.

3 Preliminary Concepts

The lattice effective properties represents lattice behavior (deformation pattern and directional stiffness) from a material perspective. Lattice, even if its characteristics stems from its geometric configuration, it can still be considered as a material. At a very long wavelength, the lattice materials can be assumed as homogeneous materials while their properties are termed as effective properties. One can then apply governing principles of classical elasticity theory to lattice materials. Hence, in this section, we briefly revise the theoretical background about the fundamental theories of classical elasticity: Hooke's Law. We also discuss various crystal symmetries and corresponding independent constants followed by relation between these constants and wave velocities.

3.1 Elasticity and Material Symmetry

In this section, we will first investigate the stress-strain relations for anisotropic materials. The in depth background about the concepts discussed here can be found in references [47–49]. The general stress-strain relation for an homogeneous elastic media with small strain approximation can be written as follows: $\sigma_{ij} = C_{ijkl}\epsilon_{kl}$, where σ and ϵ are the macroscopic stress and strain tensors, respectively, C is a fourth order stiffness tensor, and indices i,j,k,l take on values 1, 2, or 3. The equation is written in terms of index notations. The stiffness tensor C_{ijkl} with 81 elements can be reduced to a simple form as C_{ij} (known as "Voigt notation) due to the stress and strain tensors symmetry. The strain component in Voigt notation ϵ_j is defined as,

$$\epsilon_1 = \frac{\partial u_1}{\partial x_1}, \epsilon_2 = \frac{\partial u_2}{\partial x_2}, \epsilon_3 = \frac{\partial u_3}{\partial x_3}, \tag{1}$$

$$\epsilon_4 = \frac{1}{2}\left(\frac{\partial u_2}{\partial x_3} + \frac{\partial u_3}{\partial x_2}\right), \epsilon_5 = \frac{1}{2}\left(\frac{\partial u_3}{\partial x_1} + \frac{\partial u_1}{\partial x_3}\right), \epsilon_6 = \frac{1}{2}\left(\frac{\partial u_1}{\partial x_2} + \frac{\partial u_2}{\partial x_1}\right), \tag{2}$$

where u_1, u_2, and u_3 represent the displacements in the x_1, x_2, and x_3 directions, respectively. This simple form of stiffness matrix C_{ij} now has 36 stiffness matrix constants. This reduction from 81 to 36 is because of the symmetry of the stress and strain. This stiffness matrix itself is symmetric due to strain energy density symmetry and thus has only 21 independent constant. This full matrix form of the stiffness matrix is shown as,

$$\begin{bmatrix} \sigma_1 \\ \sigma_2 \\ \sigma_3 \\ \sigma_4 \\ \sigma_5 \\ \sigma_6 \end{bmatrix} = \begin{bmatrix} C_{11} & C_{12} & C_{13} & C_{14} & C_{15} & C_{16} \\ & C_{22} & C_{23} & C_{24} & C_{25} & C_{26} \\ & & C_{33} & C_{34} & C_{35} & C_{36} \\ & & & C_{44} & C_{45} & C_{46} \\ & & SYM & & C_{55} & C_{56} \\ & & & & & C_{66} \end{bmatrix} \begin{bmatrix} \epsilon_1 \\ \epsilon_2 \\ \epsilon_3 \\ \epsilon_4 \\ \epsilon_5 \\ \epsilon_6 \end{bmatrix} \tag{3}$$

This is the stress-strain relation for a most general anisotropic material that has no plane of symmetry for the material properties. It should be notated that the strain component corresponding to shear deformation are one-half of the shear strains. Natural materials often exhibits some kind of material symmetry. Such materials with symmetry planes for the material

properties will have the reduced number of independent constants. Material with specific symmetry planes and their constitutive equations are discussed below that we use later to analyze the lattice structure studied in this thesis. For detailed description of symmetry planes refer [49].

For materials having a single plane of symmetry when the symmetry plane coincides with the x_1-x_2 plane, the stress-strain relation is:

$$\begin{bmatrix} \sigma_1 \\ \sigma_2 \\ \sigma_3 \\ \sigma_4 \\ \sigma_5 \\ \sigma_6 \end{bmatrix} = \begin{bmatrix} C_{11} & C_{12} & C_{13} & 0 & 0 & C_{16} \\ & C_{22} & C_{23} & 0 & 0 & C_{26} \\ & & C_{33} & 0 & 0 & C_{36} \\ & & & C_{44} & C_{45} & 0 \\ & & SYM & & C_{55} & 0 \\ & & & & & C_{66} \end{bmatrix} \begin{bmatrix} \epsilon_1 \\ \epsilon_2 \\ \epsilon_3 \\ \epsilon_4 \\ \epsilon_5 \\ \epsilon_6 \end{bmatrix} \tag{4}$$

Material with two orthogonal symmetry planes, the stress-strain relation is:

$$\begin{bmatrix} \sigma_1 \\ \sigma_2 \\ \sigma_3 \\ \sigma_4 \\ \sigma_5 \\ \sigma_6 \end{bmatrix} = \begin{bmatrix} C_{11} & C_{12} & C_{13} & 0 & 0 & 0 \\ & C_{22} & C_{23} & 0 & 0 & 0 \\ & & C_{33} & 0 & 0 & 0 \\ & & & C_{44} & 0 & 0 \\ & & SYM & & C_{55} & 0 \\ & & & & & C_{66} \end{bmatrix} \begin{bmatrix} \epsilon_1 \\ \epsilon_2 \\ \epsilon_3 \\ \epsilon_4 \\ \epsilon_5 \\ \epsilon_6 \end{bmatrix} \tag{5}$$

These are "orthotropic materials" with 9 independent stiffness matrix constants. All lattice materials are atleast orthotropic by virtue of their sym-

metries about principal axes. It should be noted that the stiffness matrix diagonal elemnts can not be negative however off-diagonal elements can be, which indicates negative Poisson's ratio. Further if the two symmetry planes are identical even after the material is rotated by 90 degrees, a material in that case is called as "tetragonal symmetric material". The stress-strain relation in that case is:

$$\begin{bmatrix} \sigma_1 \\ \sigma_2 \\ \sigma_3 \\ \sigma_4 \\ \sigma_5 \\ \sigma_6 \end{bmatrix} = \begin{bmatrix} C_{11} & C_{12} & C_{13} & 0 & 0 & 0 \\ & C_{11} & C_{13} & 0 & 0 & 0 \\ & & C_{33} & 0 & 0 & 0 \\ & & & C_{44} & 0 & 0 \\ & & SYM & & C_{44} & 0 \\ & & & & & C_{66} \end{bmatrix} \begin{bmatrix} \epsilon_1 \\ \epsilon_2 \\ \epsilon_3 \\ \epsilon_4 \\ \epsilon_5 \\ \epsilon_6 \end{bmatrix} \tag{6}$$

If the material properties are independent of direction in one plane then such materials are referred to as "transversely isotropic materials" and the stress-strain relation in that case is:

$$\begin{bmatrix} \sigma_1 \\ \sigma_2 \\ \sigma_3 \\ \sigma_4 \\ \sigma_5 \\ \sigma_6 \end{bmatrix} = \begin{bmatrix} C_{11} & C_{12} & C_{13} & 0 & 0 & 0 \\ & C_{11} & C_{13} & 0 & 0 & 0 \\ & & C_{33} & 0 & 0 & 0 \\ & & & C_{44} & 0 & 0 \\ & & SYM & & C_{44} & 0 \\ & & & & & (C_{11}-C_{12})/2 \end{bmatrix} \begin{bmatrix} \epsilon_1 \\ \epsilon_2 \\ \epsilon_3 \\ \epsilon_4 \\ \epsilon_5 \\ \epsilon_6 \end{bmatrix} \tag{7}$$

If the material has a 45 degree symmetry in all planes, then it has a "cubic

symmetry" and its stiffness matrix has only 3 independent constant as shown below:

$$\begin{bmatrix} \sigma_1 \\ \sigma_2 \\ \sigma_3 \\ \sigma_4 \\ \sigma_5 \\ \sigma_6 \end{bmatrix} = \begin{bmatrix} C_{11} & C_{12} & C_{12} & 0 & 0 & 0 \\ & C_{11} & C_{12} & 0 & 0 & 0 \\ & & C_{11} & 0 & 0 & 0 \\ & & & C_{44} & 0 & 0 \\ & & SYM & & C_{44} & 0 \\ & & & & & C_{44} \end{bmatrix} \begin{bmatrix} \epsilon_1 \\ \epsilon_2 \\ \epsilon_3 \\ \epsilon_4 \\ \epsilon_5 \\ \epsilon_6 \end{bmatrix} \tag{8}$$

The lattice structure discussed in this thesis are anisotropic and their symmetry is governed by the geometry of lattice unit cell. The lattice properties are thus going to be direction dependent and will have more than two independent stiffness constant. Only isotropic materials has two independent stiffness matrix constants.

3.2 Plane Wave Propagation and Christoffel's Equation

In this section, we will use wave equation to derive Christoffel's equation that relates the wave velocity and material properties. We will use this equation to reverse engineer the properties of our lattice material based on wave velocities. The 3D wave equation for an elastic wave within an anisotropic material in index notations is given as:

$$\frac{\partial \sigma_{ij}}{\partial x_j} = \rho \frac{\partial^2 u_i}{\partial t^2}, \tag{9}$$

where σ denotes the stress tensor, $\mathbf{u}$, the displacement vector and ρ, mass density of the material. Substituting the stress-strain relation and strain compatibility relation, discussed in previous section, we arrive at,

$$\frac{\partial C_{ijkl}}{\partial x_j}\frac{\partial u_k}{\partial x_l} + C_{ijkl}\frac{\partial^2 u_k}{\partial x_j \partial x_i} = \rho\frac{\partial^2 u_i}{\partial t^2}, \tag{10}$$

As discussed previously, we will be dealing with spatially homogeneous material. We will assume that effective medium of the lattice materials is continuous and homogeneous. In that case, there is no C_{ijkl} dependence on spatial coordinates. The first term in the above equation is then trivial and the equation reduces to,

$$C_{ijkl}\frac{\partial^2 u_k}{\partial x_j \partial x_i} = \rho\frac{\partial^2 u_i}{\partial t^2}, \tag{11}$$

We will now consider a point source that generates a spherical wave far away from the material. With this assumption, by the time wave reaches material it is a plane wave and we can assume plane wave solution in our wave equation. The particle displacement, u_m of an harmonic plane wave propagating in an anisotropic medium is given as:

$$u_m = U_m e^{[i(k_n x_n - \omega t)]}, \tag{12}$$

where k_n denotes the wavenumber for the x_n direction that is the direction of wave propagation and ω, the frequency while $U - m$, the amplitude of

the particle displacement in the x_m direction that is the direction of particle displacement also called as wave polarization. In case of an elastic medium, there exists two types of wave polarization: Longitudinal and Transverse. The particle displacement is parallel to propagation direction in the former case whereas in later one the particle displacement is perpendicular to wave propagation direction. By implementing harmonic wave displacement function we get,

$$k^2 C_{ijkl} n_j n_l u_k = \rho \omega^2 u_i, \tag{13}$$

where we define the unit direction vector as

$$\mathbf{n} = n_{x_1} \hat{\imath} + n_{x_2} \hat{\jmath} + n_{x_3} \hat{k}, \tag{14}$$

This is the Christoffel equation, which can also be written as an eigenvalue problem discussed later in section 6.

4 Description of Lattice Geometries

The unit cells of lattice geometries studied are shown in Fig. 2. The lattices of interest are cubic [50], foam, octet [51], and Kelvin [50,51] of cubic symmetry; hexagonal [5] of transversely isotropic symmetry; and a modified octet (termed 'octet-A') and bowtie [52] of tetragonal symmetry. An in-depth analysis of the bowtie lattice, and the way its wave velocities and effective properties evolve over a range of internal cell angle, α, (Fig. 2e) that cause the lattice to vary from negative to positive Poisson's ratio is presented.

The parent material of the lattices is modeled as polycarbonate with E = 1 GPa, $\nu = 0.35$, $\rho = 1097$ kg/m^3, and is considered isotropic. The lattice constant, L, is 8 mm, 7 mm and 4 mm for foam, bowtie, and all other remaining lattices, respectively, and is kept constant throughout the geometric parameterization. The geometric parameterization includes internal cell angle, α, for the bowtie lattice and truss thickness, t, for all other lattices (Fig. 2d-e). The internal cell angle is varied from 55° to 90° with an interval of 2.5°, and truss thickness is varied from 0.1 to 1 mm at an interval of 0.1 mm. The internal cell angle of bowtie lattice is studied in order to evaluate the lattice properties that span a negative to positive Poisson's ratio.

By studying the geometry of the lattices, we can determine the symmetry of the effective material. Fig. 3 shows planes of symmetry for cubic, tetragonal and transversely isotropic materials in general. From the unit cell geometry of bowtie lattice (Fig. 2b), it can be seen that it has 45° symmetry only in the XY plane, making it a tetragonal structure. We design another tetragonal unit cell by modifying the cubically symmetric octet lattice in such a way that it will have 45° symmetry only in the XY plane. To do so, we remove four internal horizontal trusses (Fig. 2c), and we refer to this unit cell as

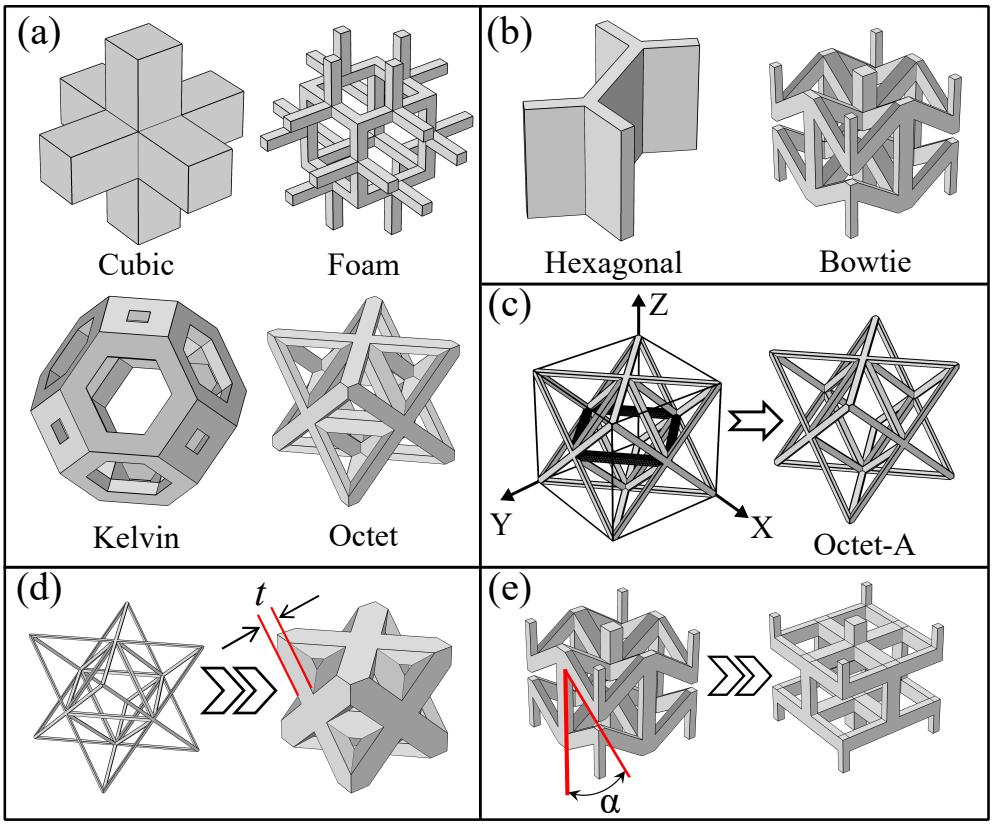

Figure 2: Unit cells of (a) cubic symmetry lattices, and (b) lower symmetry lattices. (c) Transformation of cubically symmetric octet lattice into a tetragonal 'octet-A' lattice by removing four trusses (highlighted in magenta). The coordinate system shown is used for all unit cell configurations. The effect of lattice geometry parameterization is shown for (d) truss thickness, t, of octet lattice, and (e) internal cell angle, α, of bowtie lattice.(Reproduced from [https://doi.org/10.1121/1.5091690], with the permission of AIP Publishing)

the 'octet-A' lattice. The hexagonal unit cell has infinite number of elastic symmetries in the XY plane, thus it is transversely isotropic with Z-direction being the out-of-plane axis. These unit cells are repeated spatially in 3D space to form an infinite array of lattice materials as shown in Fig. 4.

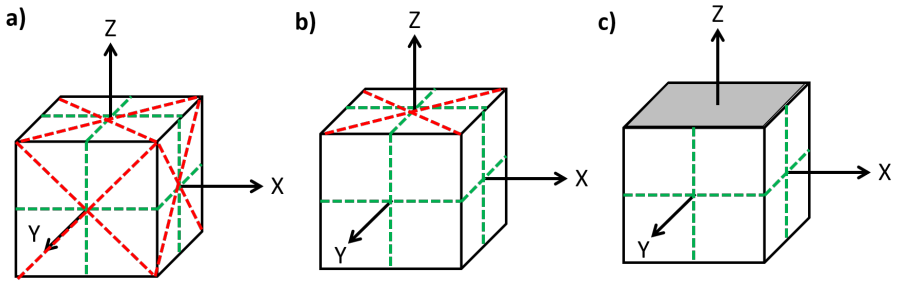

Figure 3: Planes of symmetry of a) cubic b) tetragonal and c) transversely isotropic material. The red and green dashed line indicates 45° and 180° (orthotropic) plane of symmetry. Gray shaded region is isotropic plane with infinite number of planes of symmetry.

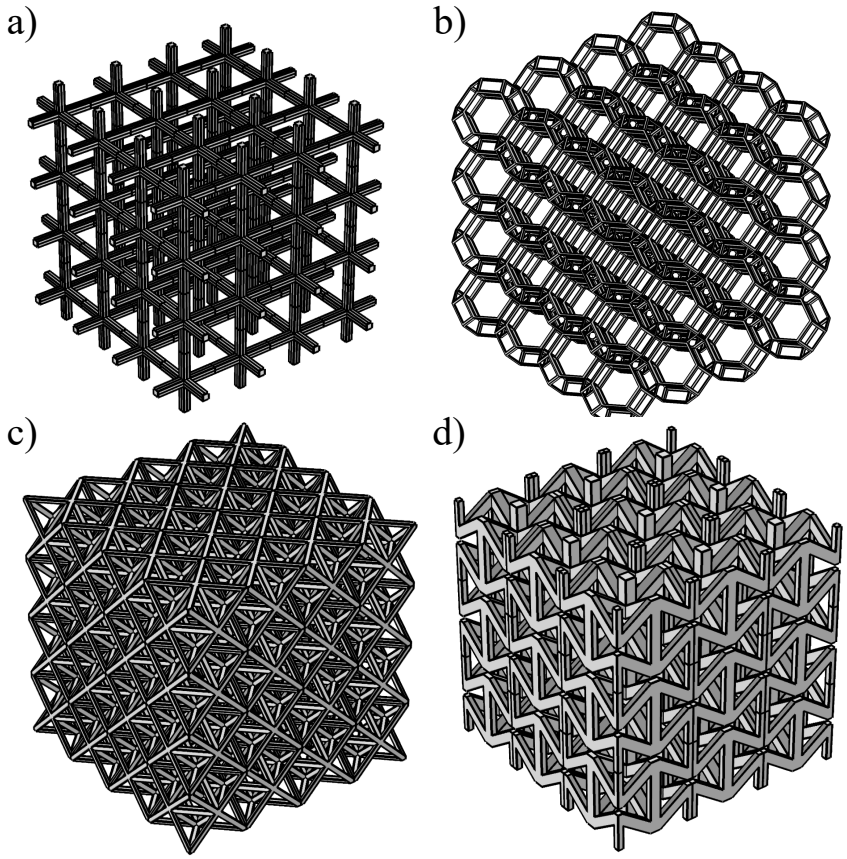

Figure 4: Array of (a) cubic, (b) Kelvin, (c) octet, and (d) bowtie lattice. These are are created by spatial three-dimensional repetition of the unit cells.

5 Elastostatic Homogenization

In this section, we discuss the elasto-static homogenization method to evaluate effective properties of lattice material. We used these results to validate our results obtained from Bloch-wave homogenization method. Homogenization technique is widely used to evaluate the effective properties of combined materials. In this method the structure composed of different materials is assumed as an equivalent effective continuum with same overall geometric dimension; this is done so as to treat the structural response as a smooth function of its geometry as illustrated in Fig. 5. In other words, one can say that effective continuum will be the combined effect of weighted contribution of parent materials. In case of lattices, the same theory can be applied while the second material can be considered as an air having extremely compliant mechanical properties. The weighted contribution because of the second material in lattices thus will be negligible.

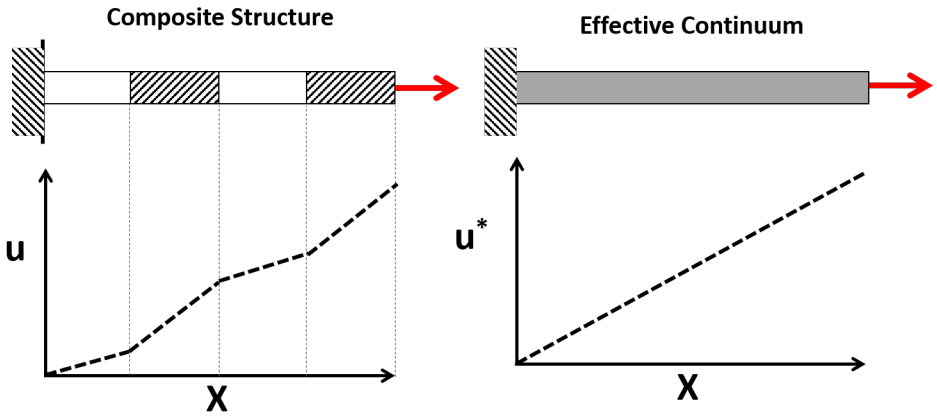

Figure 5: Concept of Equivalent Continuum: white and gray shaded regions indicates two different materials and u is the response of the material under uniaxial loading

We first calculate the effective properties of the lattice materials using ap-

propriate static boundary conditions within a finite element method framework. In an FE analysis, the PBC can be easily applied as nodal displacement constraints that automatically guarantee traction continuity on the RVE boundaries [9]. This continuity periodic boundary condition is essential since material that is periodic before deformation must also be periodic after deformation [37]. To do this, we analyze a single unit cell and apply both periodic boundary conditions on all unit cell boundaries and classical boundary conditions of uniform displacement along the direction of interest. The apparent properties of the unit cell obtained under classical boundary conditions (displacement, traction or mixed) represent effective properties when the periodicity of the structure is incorporated [2, 53]. We define the periodic boundary condition as

$$u_i^{+\hat{n}} - u_i^{-\hat{n}} = \epsilon_{ij} \left(x_j^{+\hat{n}} - x_j^{-\hat{n}} \right), \tag{15}$$

where u is the average displacement of the faces defined by unit normal vector, $\hat{n}$. Positive and negative signs indicate that the normal vectors representing a pair of periodic faces are opposite to each other, one being a source and other being a destination of the periodicity. ϵ and x are the macroscopic strain and nodal coordinates, respectively, in given i and j direction. For the above-mentioned elastostatics boundary value problem, the constitutive equation for small strain deformation is $\sigma_{ij} = C_{ijkl}\epsilon_{kl}$, where σ and ϵ are the macroscopic stress and strain tensor, respectively, C is a fourth order stiffness tensor, and indices i,j,k,l take on values 1, 2, or 3. Our aim is to solve for this stiffness tensor and thereby evaluate the effective properties.

To evaluate the stiffness tensor constants of an effective continuum associated with uniaxial loading, we apply uniaxial displacement on opposing faces

and then evaluate macroscopic stresses as

$$\sigma^* = \frac{\int_{A^*} dR}{\int_{A^*} dA^*}, \tag{16}$$

where σ^* is the effective stress acting on the effective surface area, A^*, on which the displacement, u, is applied, and R is the reaction force on that surface [2]. Effective strain, ϵ^*, is evaluated as the ratio of applied displacement, u, to the original length in that direction. We then use these macroscopic (or effective) stress-strain values in the constitutive equation (stiffness tensor, C, is now reduced to 3 non-zero independent constants due to uniaxial loading and periodic BCs [54]) to evaluate the corresponding stiffness tensor constant. For example, when the displacement is applied along the X-direction with 3D periodicity then the stiffness tensor constants C^*_{11}, C^*_{12}, and C^*_{13} are evaluated. We replicate this same procedure in other two directions, independently, to evaluate remaining stiffness tensor constants (C^*_{22}, C^*_{23}, and C^*_{33}). We then simulate pure shear loading (displacement based) in all planes, independently, to evaluate the stiffness tensor constants corresponding to shear moduli (C^*_{44}, C^*_{55}, and C^*_{66}). To simulate pure shear, we apply equal and opposite displacement on a pair of two opposite faces of the unit cell with planar boundary conditions on the third pair. We evaluate corresponding effective shear stress using Eq. (16) and effective shear strain based on the angle of deformation. The boundary conditions discussed here are shown in Fig. 6

We performed elastostatic homogenization using commercial COMSOL Multiphysics (4.3b) software with standard physics controlled fine mesh. We used symmetric meshing on periodic faces for computational efficiency. We applied continuity periodic boundary conditions in three directions to sim-

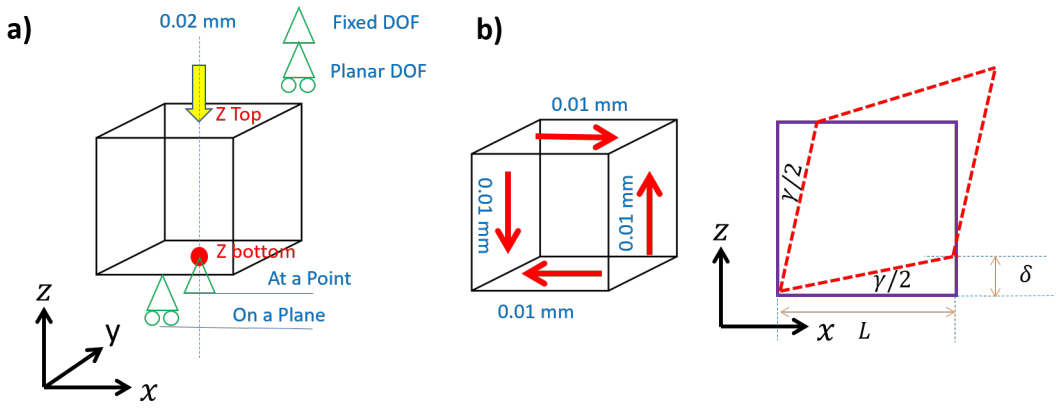

Figure 6: Boundary conditions for elasto-static homogenization - a) Uniaxial loading, and b) Pure shear loading. Addition to shown boundary conditions, periodic boundary conditions are also applied on each side.

ulate geometric periodicity of the lattices. The displacement and planar boundary conditions were applied using prescribed displacement. The strain values within structure was limited within proportinality limit even though the analysis was within linear environment. For cubic symmetry lattices, two static simulations were needed to obtain the stiffness tensor with 3 independent constants, whereas for transverse isotropy and tetragonal symmetric lattice, four static simulations, two with uniaxial loadings and two with shear loading, were required to obtain 6 and 5 independent stiffness tensor constants, respectively [49]. To validate the obtained stiffness tensor, we check the stiffness tensor positive definiteness governed by positive definiteness of the strain energy density. For a tetragonal symmetric material following necessary and sufficient conditions were verified [55, 56]:

$C_{11} > \|C_2\|$

$2{C_{13}}^2 < C_{33}(C_{11} + C_{12})$

$C_{44} > 0$

$C_{66} > 0$

6 Bloch-wave Homogenization

In this section, we apply the Bloch theorem to the elastostatics, where the structure of interest is periodic in nature, and its unit cell, when tessellated, will form an infinitely periodic structure. Bloch generalized Floquet's 1D mathematical result on to a 3D system to obtain the wave function that relates a simple plane wave with the periodicity of the structure [57]. We apply this concept to analyze the unit cell of an infinite lattice that eventually tells us the behavior of the entire structure.

We consider a lattice structure with two points, P and Q, with position vectors, $\vec{r}_P$ and $\vec{r}_Q$, respectively, at a distance from each other such that

$$\vec{r}_Q = \vec{r}_P + \vec{r}. \tag{17}$$

Here, we write position vector, $\vec{r}$, in terms of the lattice constant as $\vec{r} = n_i \hat{e}_i$, where n_i is unit cell number in the direction of unit vectors, $\hat{e}_i$ (refer Fig. 7). Assuming plane wave propagation, Bloch's theorem relates the displacement of any other point, Q, in any cell as

$$\vec{u}_Q(\vec{r}_Q, t) = \vec{u}_P e^{-i\left[\vec{k}(\vec{r}_Q - \vec{r}_P)\right]}, \tag{18}$$

where $\vec{k}$ is a wave vector. Since $\vec{r}_Q$-$\vec{r}_P$ is simply a function of the periodicity constant, we can identify the displacement of any other point within the lattice structure based on the analysis of a single unit cell for a known wave vector. We assume $\vec{k}$ is real, i.e. we neglect the attenuation in this analysis.

One can further reduce the computational problem by restricting wave vectors to the edges of the irreducible Brillouin zone (IBZ) [58] for band

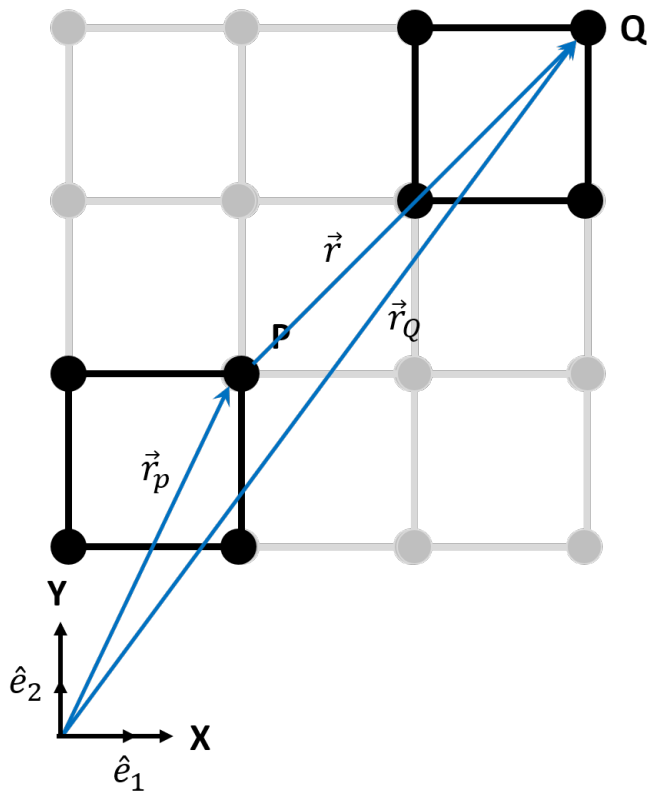

Figure 7: Lattice configurations used to to develop Bloch-wave equations. Square geometry at lower-left corner is our unit cell of interest.

gap analysis of periodic structures [5]. However, in this paper, we analyze the long-wavelength wave propagation only along certain directions that we decide based on the number of independent stiffness tensor constants governed by the symmetry of the unit cell geometry. We then use the equations of motion to solve the eigenvalue problem of the propagating wave for the frequency, ω, at each combination of wave vectors. We obtain the dispersion curves (ω-k space) in the long wavelength limit, where the phase and group velocities are equal (denoted 'V' hereafter) and are independent of frequency [47]. We use this wave velocity information to analyze the lattice structures.

We determine the stiffness tensor constants, C^*_{ijkl}, of an effective continuum

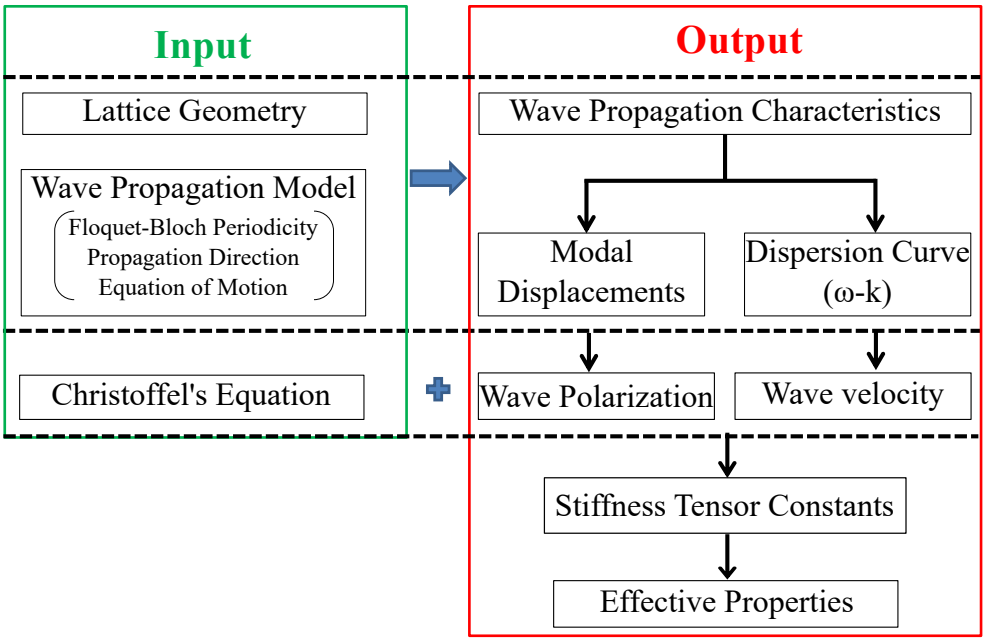

Figure 8: Schematic of Bloch-wave homogenization method. (Reproduced from [https://doi.org/10.1121/1.5091690], with the permission of AIP Publishing)

from the obtained wave velocities, V, through the Christoffel's equation [59]:

$$\Gamma_{ik} = C^*_{ijkl} n_j n_l, \tag{19}$$

$$\left(\Gamma_{ik} - \delta_{ik}\rho^* V^2\right) P_m = 0, \tag{20}$$

where Γ is the acoustic tensor, ρ^* is the effective density, n_i is the direction cosine, P_m is the component of the unit vector in the displacement direction and δ_{ik} is the Kronecker delta function. As each stiffness tensor constant is related to a particular type of propagating wave, identifying the wave polarization is essential (i.e. n_i and P_m must be known). In an effective elastic continuum, there exist three propagating waves within any structure:

one longitudinal and two transverse. Generally, longitudinal velocities are higher than the transverse for an isotropic structure [5] and are independent of propagation direction. This is not always the case and it is non-trivial to identify the wave polarization within anisotropic structures. We also observe the existence of 'quasi' waves when the wave propagates along any direction other than the principal axes in an anisotropic plane, and that the particle displacement is neither parallel nor perpendicular to the wave propagation direction [48, 60]. Thus, we evaluate the propagating modal displacements to differentiate between the longitudinal and transverse waves. Further, for anisotropic structures, the two transverse velocities may not be equal, hence we use the wave propagation characteristics corresponding to a crystal symmetry in conjunction with the modal displacements and dispersion curves to identify the wave polarization.

This Bloch-wave homogenization method for effective material property evaluation is summarized in Fig. 8. We developed our wave propagation model within COMSOL Multiphysics (4.3b) using Floquet-Bloch periodic boundary conditions. We used physics controlled symmetric fine meshing for all our simulations with a very small range of wave vector ($< 1\%$ of the lattice constant (1/m)) to ensure the applicability of effective continuum theory in long wavelength limit. We extracted the first 3 modes that correspond to the lowest longitudinal and two transverse waves of the lattice structure and calculated a best fit using least-squares regression to extract the wave velocities (Fig. 9). We used volume averaged modal displacement along principal directions to identify the mode shapes and wave polarization.

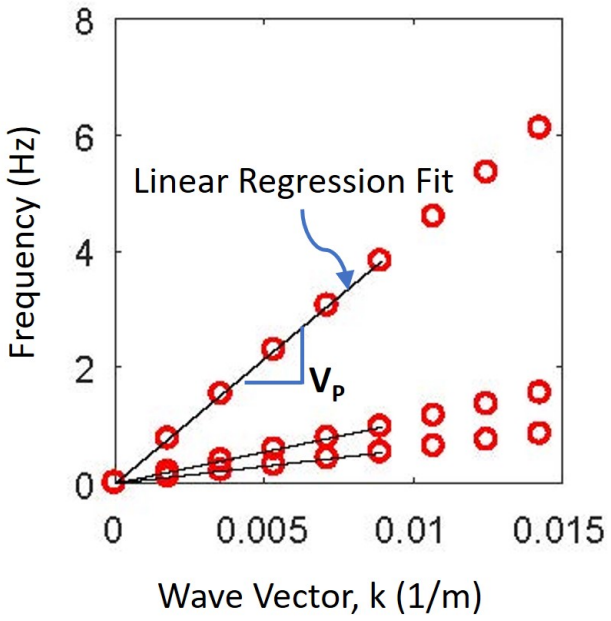

Figure 9: First three dispersion curve representing one longitudinal and two transverse wave. A best linear regression fit is done to evaluate slope of the curves. It can be seen that the the linear relationship is valid only for small wave vector values. This curve do not inform about the polarization of the wave.

7 Effective Properties of Cubic Symmetry Lattices

In this section, we present the Bloch-wave homogenization results of cubic symmetry lattices, using the octet lattice as an example case. By virtue of its geometry, the octet lattice has cubic symmetry and therefore three independent effective stiffness tensor constants: C_{11}, C_{12}, and C_{66}. The asterisk sign, which represents effective property has been dropped hereafter for convenience. These constants are related to corresponding wave velocities through following reduced form of Christoffel's equation:

$$V_{xx} = \sqrt{C_{11}/\rho}, \tag{21}$$

$$V_{xy} = V_{xz} = \sqrt{C_{66}/\rho}, \tag{22}$$

$$2\rho V_{45}^2 = (C_{11} + C_{66}) \pm (C_{12} + C_{66}), \tag{23}$$

where for V_{ij}, i indicates the direction of wave propagation and j indicates the direction of particle displacement. For V_ϕ, ϕ indicates the wave propagation angle with respect to principal axis. We evaluate the effective density, [3] ρ (asterisk dropped for convenience) based on the relative volume of the lattice and actual density of the parent bulk material. We use wave velocities along principal directions i.e. longitudinal and transverse velocities to identify the stiffness tensor diagonal elements, C_{11} and C_{66} using Eq. (21) and Eq. (22), respectively. The off-diagonal stiffness tensor constant can be calculated from waves propagating within any plane within the range of $0° < \phi < 90°$ [59]. For

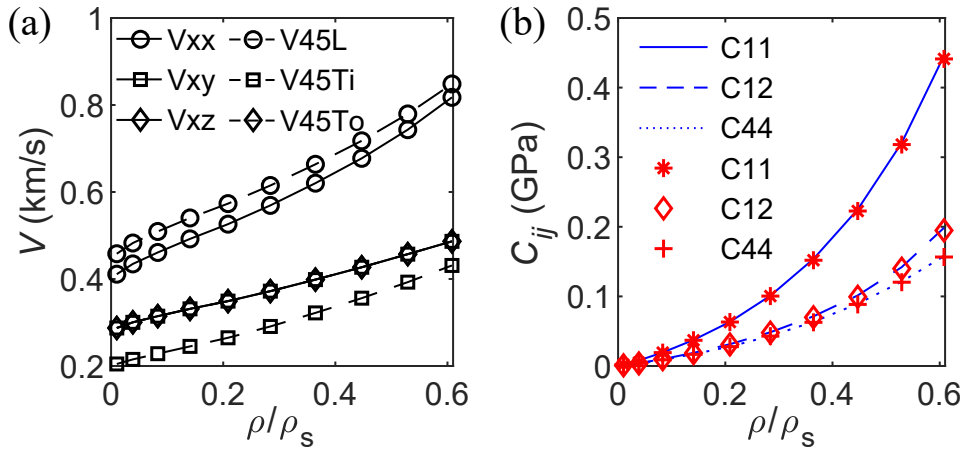

Figure 10: Octet lattice (a) wave velocities (note: $V_{xy} = V_{xz} = V_{45To}$) and (b) independent stiffness tensor constants evaluated from static (red markers) and Bloch-wave (blue lines) homogenization method. (Reproduced from [https://doi.org/10.1121/1.5091690], with the permission of AIP Publishing)

simplicity of algebraic calculation, we select wave propagation at 45° in the XY plane (or 1-2 plane). We evaluate the off-diagonal constant using Eq. (23) based on either longitudinal or in-plane transverse velocity, where the sign is selected according to the type of polarization: positive for longitudinal wave and negative for in-plane transverse wave [59].

The wave velocities and stiffness tensor constants of the octet lattice derived from Bloch-wave homogenization are shown in Fig. 10 with respect to relative density (lattice density normalized by bulk density). The evaluated stiffness tensor constants agree well with the static homogenization results. From the wave velocity results, one can observe that the transverse velocities are identical ($V_{xy} = V_{xz}$) when waves propagate along the principal direction but different ($V_{45Ti} \neq V_{45To}$, where Ti and To stands for in-plane and out-of-plane transverse polarization, respectively) when waves propagate at an angle to the principal axes. This information is also useful in identifying the lattice symmetry. The relation between the in-plane transverse wave veloc-

ities along different directions ($V_{xy} > V_{45Ti}$) indicates that the octet lattice is stronger in shear along the principal direction. On the other hand, the relation between the longitudinal wave velocities along different directions ($V_{45L} > V_{xx}$, where L indicates longitudinal polarization) indicates that the octet lattice is stronger in compression along the 45° axis.

We apply Bloch-wave homogenization to the cubic, foam and Kelvin lattices, and their effective properties along with octet lattice are shown normalized with respect to properties of the bulk material (Fig. 11). Results of the Kelvin lattices are presented only up to truss thickness of 0.8 mm since the geometry changes at higher values. We show the relationship between the logarithm of the relative modulus and relative density of these lattices for low relative densities in Fig. 11d-e. We then calculate the polynomial best fit of initial five data points through least-squares regression and obtain the power law relationship between the actual quantities as $E/E_s \propto (\rho/\rho_s)^m$ and $G/G_s \propto (\rho/\rho_s)^n$. The exponents, m and n, of the power laws correspond to the slopes of the lines in log plots. An exponent of $m, n = 1$ signifies that the geometry is stretch-dominant, while an exponent of $m, n = 2$ indicates that the geometry is bending-dominant [8]. We see that for the lower values of relative densities, $E/E_s \propto \rho/\rho_s$ and $G/G_s \propto \rho/\rho_s$ for the octet lattice as also shown theoretically by Deshpande et al. [33], whereas for the Kelvin lattice, $E/E_s \propto (\rho/\rho_s)^2$ and $G/G_s \propto (\rho/\rho_s)^2$ as shown experimentally by Zheng et al. [51]. The foam lattice effective properties also scales with $(\rho/\rho_s)^2$, whereas cubic lattice shows combined behavior with $E/E_s \propto \rho/\rho_s$ under uniaxial compression but $G/G_s \propto (\rho/\rho_s)^2$ under shear loading. Consistent with much prior work, at lower relative densities, the octet lattice is stretch dominant [8, 51], the foam and Kelvin lattices are bending dominant [51], and the cubic lattice is stretch dominant in compression but bending dominant in shear. As the

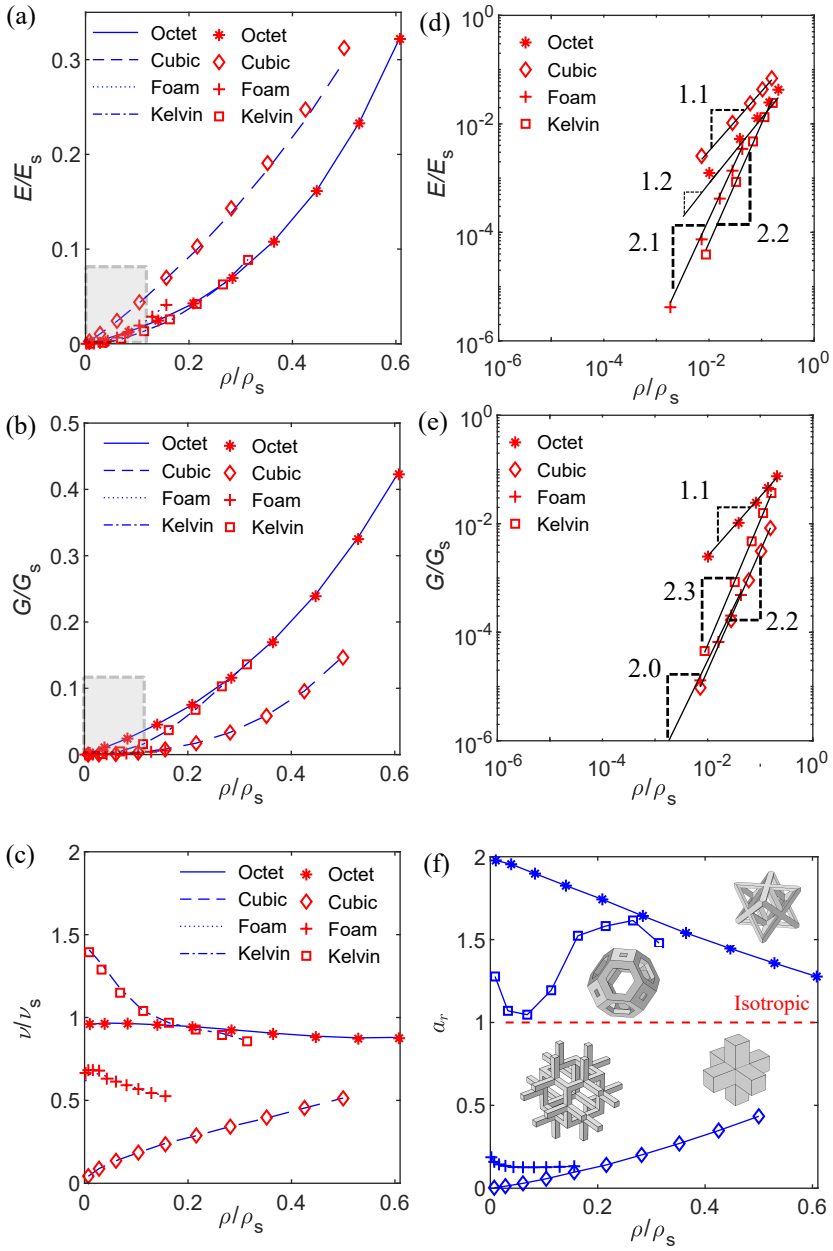

Figure 11: Normalized effective mechanical properties (a) uniaxial modulus, (b) shear modulus, and (c) Poisson's ratio of cubic symmetry lattices. Magnified logarithmic plots of shaded area of (a) and (b) are shown in (d) and (e) for better visualization of low relative density results with numerical values indicating slopes. (f) Zener anisotropy index of cubic symmetry lattices. (Reproduced from [https://doi.org/10.1121/1.5091690], with the permission of AIP Publishing)

relative density increases, the linear relation between relative modulus and relative density of the octet lattice becomes non-linear (Fig. 11a-b) signifying

the truss bending effect during deformation. Overall, the Kelvin lattice is much weaker in uniaxial loading compared to cubic lattice as observed by Hedayati et al. [61]. However, in contrast to their shear modulus predictions, we find that the Kelvin lattice has a higher shear modulus compared to the cubic lattice (truss beam modeling and rigid vertices are possibly making the cubic lattice more shear resistant in Hedayati et al. [61]). The truss joints in the Kelvin geometry are thus stronger than in the foam and cubic geometry.

We also see that the octet lattice almost maintains a constant Poisson's ratio (Fig. 11c) at low relative densities and deviates slightly at higher relative densities. The absolute value of the octet lattice Poisson's ratio is also almost same as that of the parent bulk material, which indicates that the macroscopic deformation in octet lattice is analogous to bulk material deformation. For both cubic and foam lattices, there is a steep increase in Poisson's ratio initially, possibly due to negligible bending resistance contributing to lateral deformation. For the cubic lattice, the increase in lateral deformation is always higher than the uniaxial deformation (due to stretch dominant behavior) and thus Poisson's ratio increases throughout. Kelvin and foam lattice, due to their bend dominant characteristic, offers significant bending stiffness and thus as relative density increases, their Poisson's ratio decreases.

We compare these cubic symmetry lattices by evaluating their Zener anisotropy index [62], $a_r = 2C_{44}/(C_{11} - C_{12})$, shown in Fig. 11f. While the Zener anisotropy index is limited to cubic symmetry lattices, it gives important insights on the variation in Young's modulus with direction, which is not possible with other anisotropy indices such as the universal anisotropy index (UAI) discussed later in section 8. All the lattices have non-unity anisotropy index, and as relative density increases they tend to become more

isotropic. The cubic and foam lattices have an index less than unity, indicating their maximum Young's modulus is along the <100> direction and minimum along the <111> direction. For Kelvin and octet lattice, the case is reversed: the maximum Young's modulus is along the <111> direction and minimum along the <100> direction, as they have an index greater than unity. In other words, the cubic and foam lattices are stronger in compression along principal axes but weaker along the space diagonal (the opposite case is true for Kelvin and octet), as shown through normalized Young's modulus representational surface (of cubic and Kelvin) by Luxner et al. [50]. It should be noted that the anisotropy index of the octet lattice shown here is consistent with Berger et al. [4], where they have evaluated reciprocal of Zener anisotropy index.

8 Effective Properties of Lower Symmetry Lattices

Here, we apply the Bloch-wave homogenization to evaluate effective properties of higher anisotropy structures. We consider the tetragonal and transversely isotropic symmetry structures, which have 6 and 5 independent stiffness tensor constants, respectively.

8.1 Tetragonal Symmetry Lattices

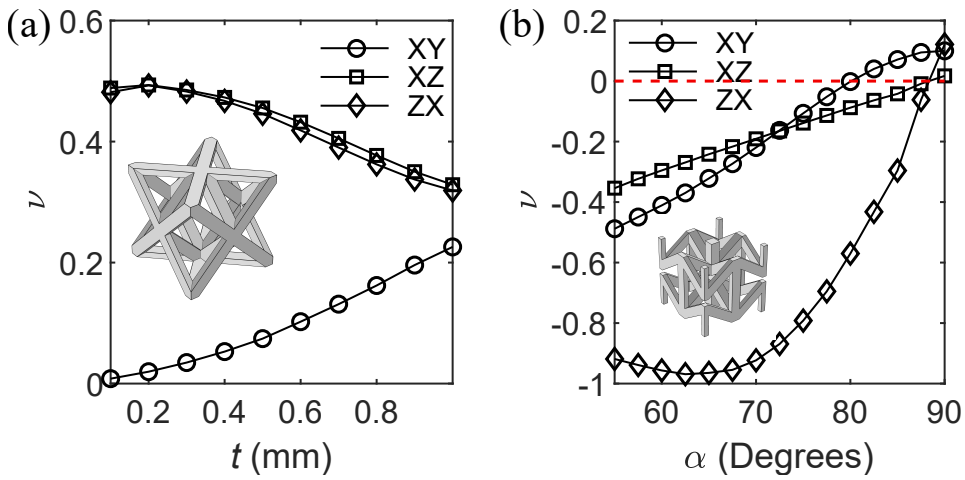

Figure 12: Poisson's ratio of (a) octet-A, and (b) bowtie lattice. Dashed red line is zero reference line. (Reproduced from [https://doi.org/10.1121/1.5091690], with the permission of AIP Publishing)

We analyze two tetragonal symmetry lattices: a new form of octet lattice, termed 'octet-A', as discussed in section 4 (refer Fig. 2c), and a bowtie lattice of tetragonal symmetry that can behave auxetically (negative Poisson's ratio) by virtue of its re-entrant truss structure. The Poisson's ratios of these two lattices obtained from static simulations are shown in Fig. 12. The octet-A lattice has positive Poisson's ratio in all planes whereas the bowtie lattice has negative Poisson's ratio that changes to positive as the internal cell angle, α, (Fig. 2e) increases. There are also instances ($87.5° \geq \alpha \geq 80°$) for the

bowtie lattice, where Poisson's ratio is negative in two planes (XZ and YZ) but positive in the other (XY). At $\alpha = 90°$, the bowtie lattice has positive Poisson's ratio throughout and thus loses its auxetic behavior. At 88° the Poisson's ratio in the XZ plane is independent of the loading direction as $\nu_{xz} = \nu_{zx}$.

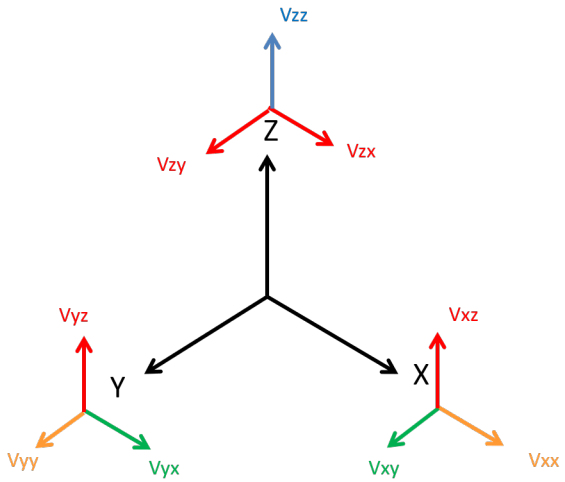

Figure 13: Tetragonal symmetry and wave velocity along material symmetry propagation direction. Similar color indicates wave velocity with same speed.

To calculate the effective stiffness tensor diagonal elements, we first calculate the wave velocities along the principal directions. To distinguish between longitudinal and transverse waves, we exploit the symmetries of the tetragonal structure, where one of the transverse X-direction waves has the same velocity as that of the transverse Z-direction wave (refer Fig. 13). Once the principal wave velocities are known, we use Christoffel's equation to evaluate the diagonal stiffness tensor constants. The diagonal constants C_{11}, C_{33}, C_{44} and C_{66} are directly related to the following wave velocities through the

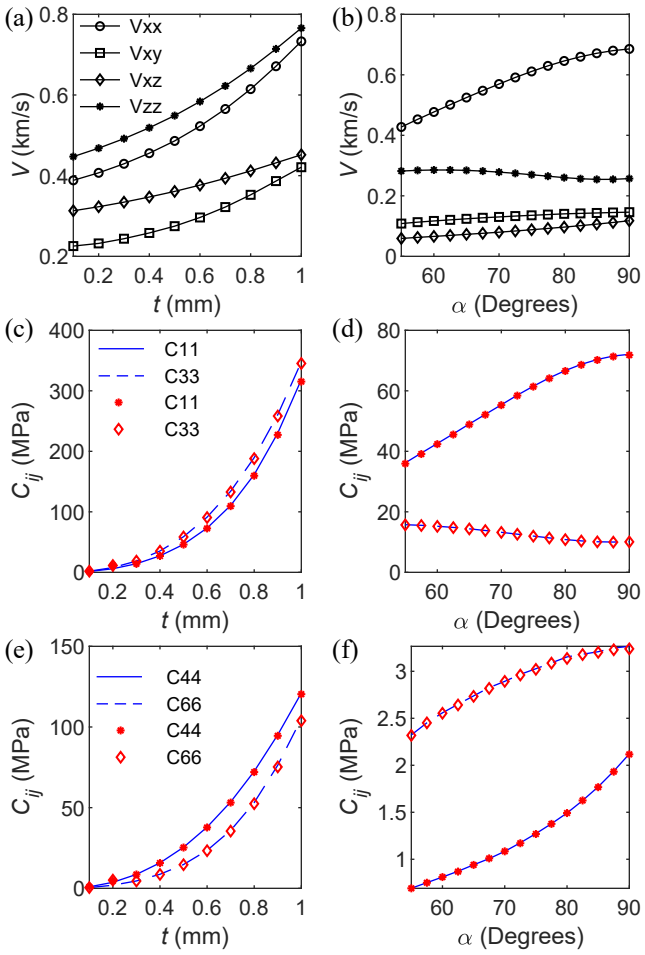

Figure 14: Principal direction wave velocities of (a) octet-A and (b) bowtie lattice. Evaluated diagonal stiffness tensor constants from static (red markers) and Bloch-wave (blue lines) homogenization of octet-A ((c) and (e)) and bowtie ((d) and (f)) lattices. Bowtie lattice plots follow the same legend scheme as that of octet-A plots.(Reproduced from [`https://doi.org/10.1121/1.5091690`], with the permission of AIP Publishing)

reduced form of Christoffel's equation:

$$V_{xx} = \sqrt{C_{11}/\rho}, \tag{24a}$$

$$V_{zz} = \sqrt{C_{33}/\rho}, \tag{24b}$$

$$V_{xy} = \sqrt{C_{66}/\rho}, \tag{24c}$$

$$V_{zx} = \sqrt{C_{44}/\rho}. \tag{24d}$$

Note that $V_{xx} = V_{yy}$, $V_{xy} = V_{yx}$, and $V_{zx} = V_{xz} = V_{zy} = V_{yz}$ by virtue of the tetragonal symmetry. The obtained wave velocities and corresponding stiffness tensor constants are shown in Fig. 14a-b and Fig. 14c-f, respectively. We see that the diagonal stiffness tensor constants calculated from Bloch-wave homogenization agree with that of static homogenization method for both the lattices.

To evaluate the off-diagonal stiffness tensor constants, we calculate velocities of waves propagating at 45° to the principal axes. The angle 45° is again selected to mathematically simplify the expressions, but any other angle ($0° < \phi < 90°$) would work [59, 63]. For waves propagating in the XY plane, there exist pure waves as properties are symmetric about 45° axes. In the case of anisotropic plane XZ, we observe one quasi-longitudinal (QL) and two quasi-transverse (QT) waves. To identify the polarization of waves propagating at an angle to the principal axis, we use global modal displacement corresponding to each mode shape. We differentiate between longitudinal, in-plane transverse, and out-of-plane transverse waves based on the dominant modal displacement corresponding to each mode (Fig. 16). The calculated wave velocities at 45° in XY (V_{45XY}) and XZ (V_{45XZ}) plane are shown in Fig. 15a-d.

The generalized form of Christoffel's equation to evaluate C_{12} of an orthotropic structure [59] for wave propagation at any angle, ϕ, in XY plane is given as

$$C_{12} = -C_{66} \pm \sqrt{\frac{2\rho V_{\phi XY}^2 - \chi_1 - \Gamma_1^2}{4n_1^2 n_2^2}}, \tag{25}$$

where $\chi_1 = C_{11}n_1^2 + C_{66}n_2^2 + C_{22}n_2^2 + C_{66}n_1^2$ and $\Gamma_1 = C_{11}n_1^2 + C_{66}n_2^2 - C_{22}n_2^2 - C_{66}n_1^2$. The wave direction vectors are defined as $n_1 = \cos\phi$ and $n_2 = \sin\phi$. The

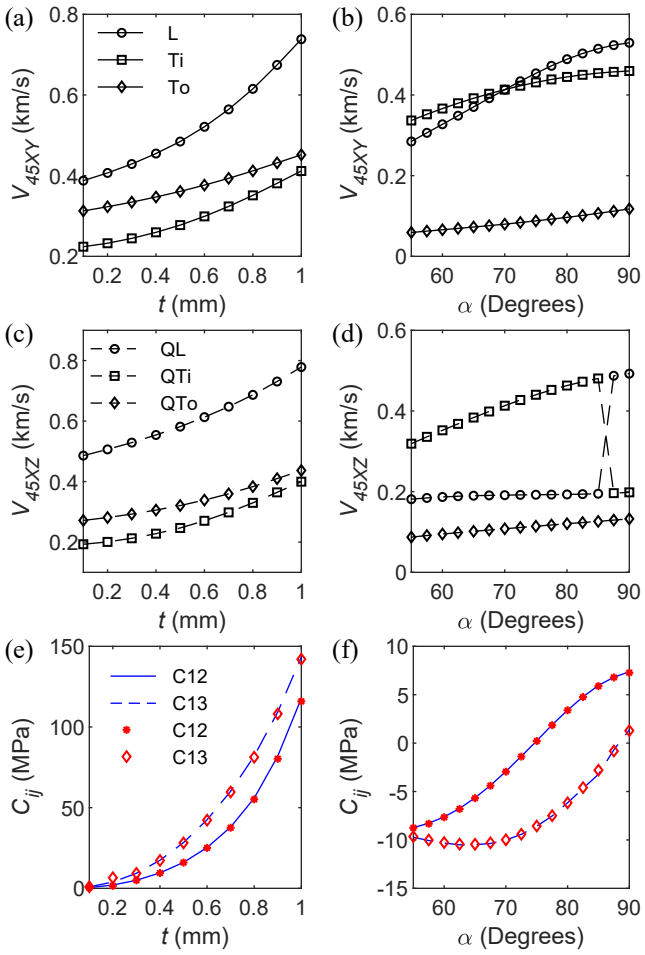

Figure 15: Non-principal directional wave velocities of octet-A lattice in (a) XY plane and (c) XZ plane; and of bowtie lattice in (b) XY plane and (d) XZ plane. L, Ti, To and Q stands for longitudinal, in-plane transverse, out-of-plane transverse and quasi waves, respectively. Resulting off-diagonal stiffness tensor constants of (e) octet-A and (f) bowtie lattice evaluated from static (red markers) and Bloch-wave (blue lines) homogenization. Bowtie lattice plots follow the same legend scheme as that of octet-A plots.(Reproduced from [`https://doi.org/10.1121/1.5091690`], with the permission of AIP Publishing)

term $V_{\phi ij}$ indicates the waves (1 longitudinal, 1 in-plane transverse and 1 out-of-plane transverse) propagating in i-j plane at ϕ° to i axis. It is important to note that either the longitudinal or in-plane transverse wave velocity can be used to identify the corresponding stiffness tensor constants [59]; the sign in front of the square root depends on the type of wave velocity used. For the

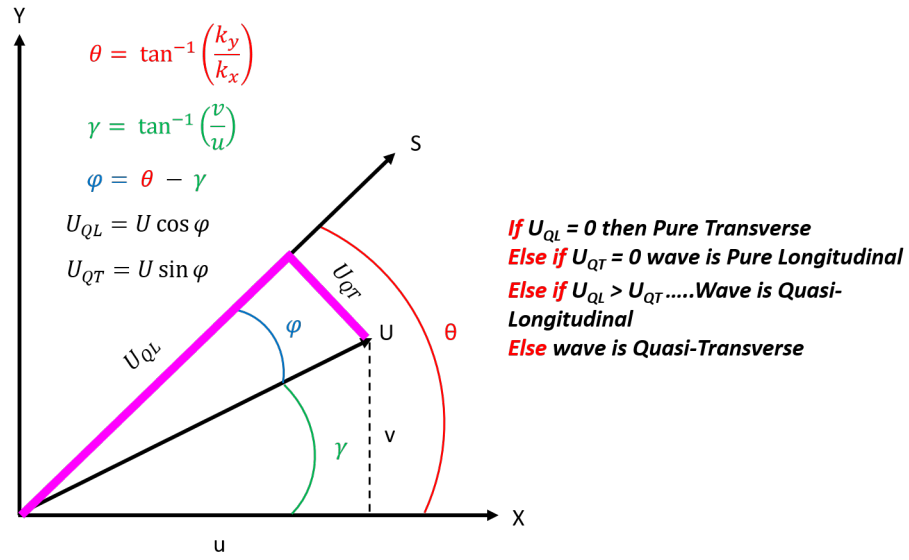

Figure 16: Algorithm to evaluate polarization of wave in an anisotropic plane. X and Y are material symmtery axis, S is wave propagation vector (or direction), and U is wave polarization vector (or particle displacement direction).

case of C_{12}, the sign of the square root is positive when using the longitudinal wave and negative when using the transverse wave; both lead to the same solution of C_{12}. Since the tetragonal structures have same properties along X and Y direction, we further simplify Eq. (25) for $\phi = 45°$ as

$$C_{12} = 2\rho V_{45XYL}^2 - C_{11} - 2C_{66}, \tag{26a}$$

$$C_{12} = -2\rho V_{45XYTi}^2 + C_{11}. \tag{26b}$$

The generalized form of Christoffel's equation to evaluate C_{13} of an orthotropic structure for wave propagation at angle ϕ in the XZ plane is given as

$$C_{13} = -C_{44} \pm \sqrt{\frac{2\rho V_{\phi XZ}^2 - \chi_2 - \Gamma_2^2}{4n_1^2 n_3^2}}, \tag{27}$$

where $\chi_2 = C_{11}n_1^2 + C_{44}n_3^2 + C_{33}n_3^2 + C_{44}n_1^2$ and $\Gamma_2 = C_{11}n_1^2 + C_{44}n_3^2 - C_{33}n_3^2 - C_{44}n_1^2$. The wave direction vectors are defined as $n_1 = \cos\phi$ and $n_3 = \sin\phi$. In the case of C_{13}, we determine the sign of the square root purely based on the sign of XZ plane Poisson's ratio (ν_{zx}) of the structure, and either of the QL or in-plane QT velocities can be used. When the lattice has a negative Poisson's ratio, the off-diagonal stiffness tensor constant must be negative, and vice versa. So, we use a positive root for octet-A lattice but for bowtie, we use a negative sign up to $\alpha < 87.5°$. For the last two angles studied, the Poisson's ratio is either zero or positive, and taking positive root is essential. The calculated off-diagonal stiffness tensor constants are shown in Fig. 15e-f. For both the octet-A and bowtie lattices, the results agree with static homogenization results. For the bowtie lattice, the off-diagonal stiffness tensor constants change signs from negative to positive signifying the change in the sign of Poisson's ratio.

The bowtie lattice exhibits an unusual wave polarization transition. Specifically, we observe a shift in faster wave polarization in both planes for the bowtie lattice (Fig. 15b,d). For smaller values of α, transverse velocity is higher, whereas for larger angles, the longitudinal velocity is higher. This shift occurs at $\alpha = 70°$ for V_{45XY}, and at $\alpha = 86.25°$ for V_{45XZ}. To illustrate this polarization shift, we show the wave velocity field of the bowtie lattice in the XY plane through an iso-frequency contour (Fig. 17). For the bowtie lattice geometry at $\alpha = 55°$, the in-plane transverse wave has a higher velocity than the longitudinal wave around 45° propagation direction. However, for $\alpha = 90$, the longitudinal wave propagates faster than the transverse wave at all propagation angles. This wave polarization transition is not present in the octet-A lattice within the parameters studied: the longitudinal wave always remains faster than the transverse waves (Fig. 15a,c).

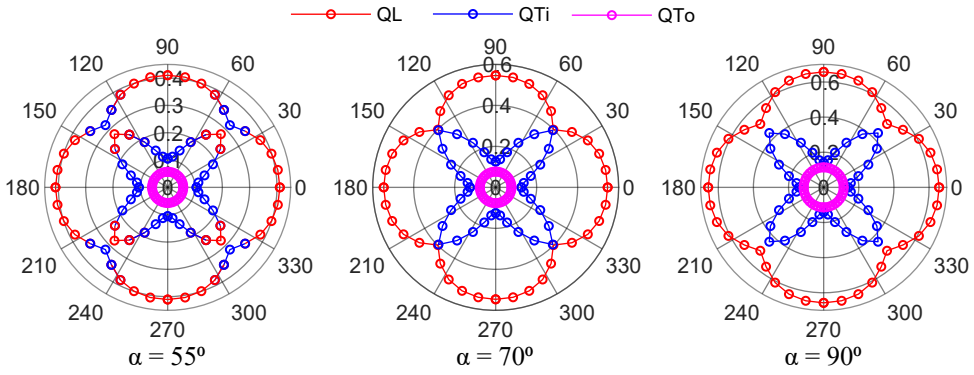

Figure 17: Iso-frequency contour of bowtie lattice wave velocities in XY plane, showing change in faster wave polarization around $\phi = 45°$ for $\alpha = 55°$. Theta in polar plot is wave propagation angle, ϕ,(in degrees) in XY plane and radius is the wave velocity, V, (in km/s). (Reproduced from [`https://doi.org/10.1121/1.5091690`], with the permission of AIP Publishing)

This anomalous behavior has been discussed by Helbig and Schoenberg [64] in a transversely isotropic structure through the analysis of slowness surfaces. In general, for anisotropic materials with $\nu > 0$, the longitudinal wave propagates with a faster velocity because $C_{12}+C_{66} > 0$ and $C_{13}+C_{44} > 0$ [64,65]. If C_{12} or C_{13} are negative (a case of auxetic structure) and greater than C_{66} and C_{44}, respectively, then the respective transverse wave is faster than the longitudinal wave. In our bowtie lattice, $C_{12} + C_{66} < 0$ when $\alpha < 70°$ and $C_{13}+C_{44} < 0$ when $\alpha < 86.25°$, thus the respective transverse waves travel faster at angles less than these values, which our results clearly show (Fig. 14f and Fig. 15b,d,f). The transverse and longitudinal wave velocities are equal at the acoustic axes or singularities [66], when $C_{12} = -C_{66}$ ($\alpha = 70°$) and $C_{13} = -C_{44}$ ($\alpha = 86.25°$). This anomalous polarization behavior has been observed in few natural materials such as calcium formate [67,68], and can be utilized in potential metamaterials applications such as mode conversion [68].

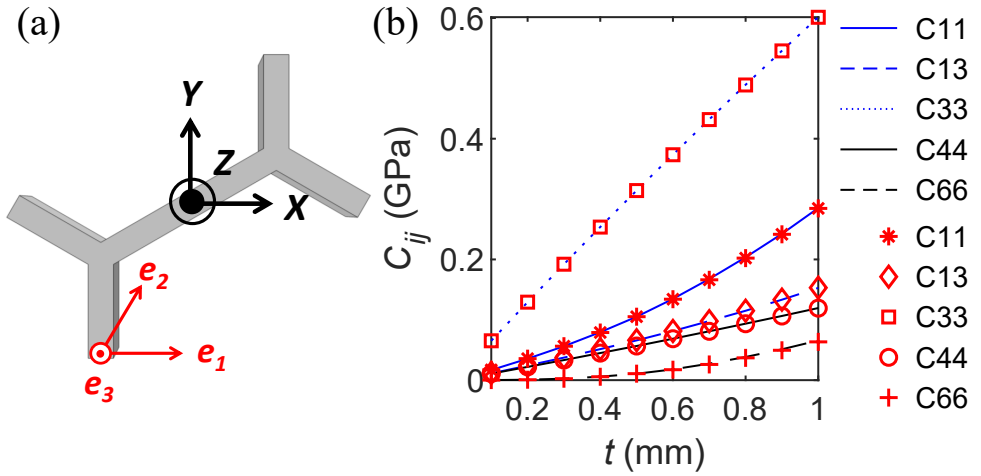

Figure 18: (a) Hexagonal cell with periodicity direction vectors, and (b) effective stiffness tensor constants evaluated through static (red markers) and Bloch-wave (blue lines) homogenization method. (Reproduced from [`https://doi.org/10.1121/1.5091690`], with the permission of AIP Publishing)

8.2 Transversely Isotropic Symmetry Lattice

The lattices discussed thus far have periodicity in three orthogonal directions. In this section, we evaluate effective properties of a hexagonal lattice that has periodicity in three directions: e_1, e_2 and e_3, of which one pair is not mutually perpendicular, e_1 and e_2, as shown in Fig. 18a. This hexagonal lattice has five independent stiffness tensor constants. We obtain identical wave propagation results in the XY plane irrespective of the direction of wave propagation, since the hexagonal lattice has one isotropic plane (XY in this case). The obtained effective properties are shown in Fig. 18b. The stiffness tensor constant C_{12} calculated from the wave velocities, V_{45XY}, using Eq. (26a) or (26b) matches with the one calculated using characteristics of transversely isotropic structure i.e. based on C_{11} and C_{66} ($C_{12} = C_{11} - 2C_{66}$).

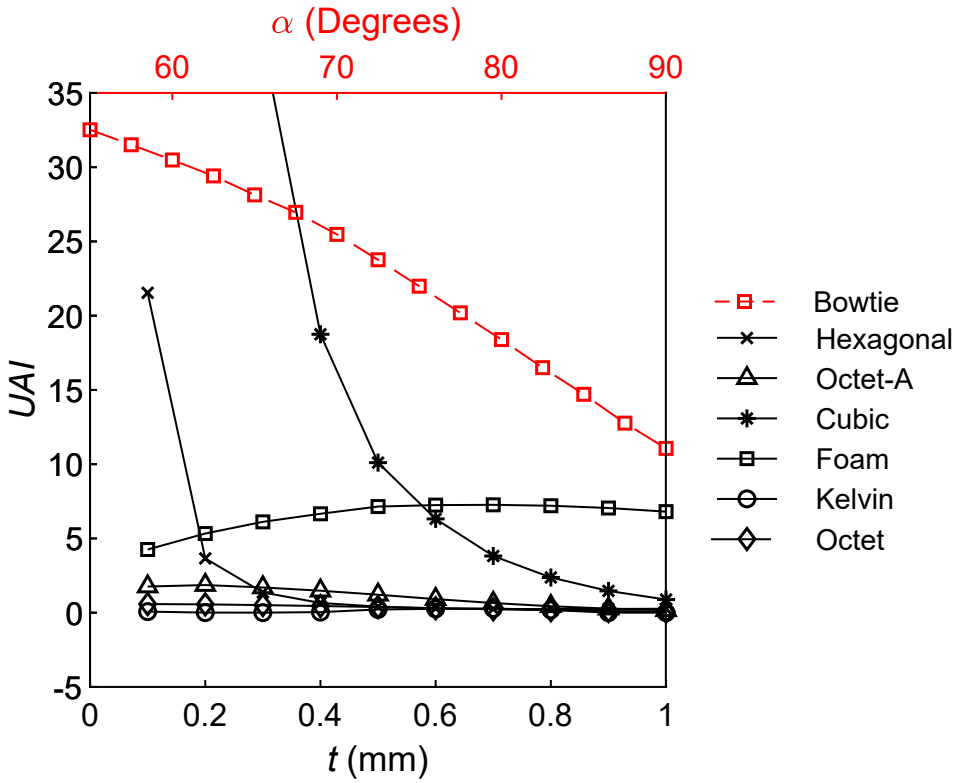

Figure 19: Universal anisotropy index of 3D lattices. Cubic lattice UAI values for truss thickness 0.1, 0.2 and 0.3 mm are 426, 95 and 38, respectively. (Reproduced from [https://doi.org/10.1121/1.5091690], with the permission of AIP Publishing)

8.3 Anisotropy Index of Lower Symmetry Lattices

In order to compare the lower symmetry lattices discussed in this section as well as the cubic lattices discussed in section 7, we evaluate Universal Anisotropy Index (UAI) [69] that quantifies the extent of anisotropy of any symmetry material. The UAI is defined as

$$A^U = 5\frac{G^V}{G^R} + \frac{K^V}{K^R} - 6. \tag{28}$$

Here, superscript V corresponds to Voigt estimates and R corresponds to Reuss estimates of bulk, K, and shear, G, modulus. Specifically,

$$G^V = \frac{1}{15}\left(C_{ijij} - \frac{1}{3}C_{iijj}\right), \tag{29a}$$

$$\frac{1}{G^R} = \frac{2}{5}\left(S_{ijij} - \frac{1}{3}S_{iijj}\right), \tag{29b}$$

$$K^V = \frac{1}{9}C_{iijj}, \tag{29c}$$

$$\frac{1}{K^R} = S_{iijj}, \tag{29d}$$

which we calculate from the effective stiffness tensor, C, and compliance tensor, S, where $S = C^{-1}$.

The dependence of UAI on geometric parameters for all lattices is shown in Fig. 19. The bowtie lattice has a higher anisotropy than both octet-A and hexagonal, whereas hexagonal is much closer to the UAI value of 0 (zero UAI indicates isotropic behavior as opposed to unity for Zener anisotropy index) indicating more isotropic behavior than others. There is a sudden shift in the extent of anisotropy for hexagonal lattice (also for cubic lattice) as truss thickness increases from very small thicknesses. This is due to the fact that at very low truss thickness the bending resistance from lattice trusses is negligible, which becomes more prominent as thickness increases.

9 Effective Properties of Composite Structures

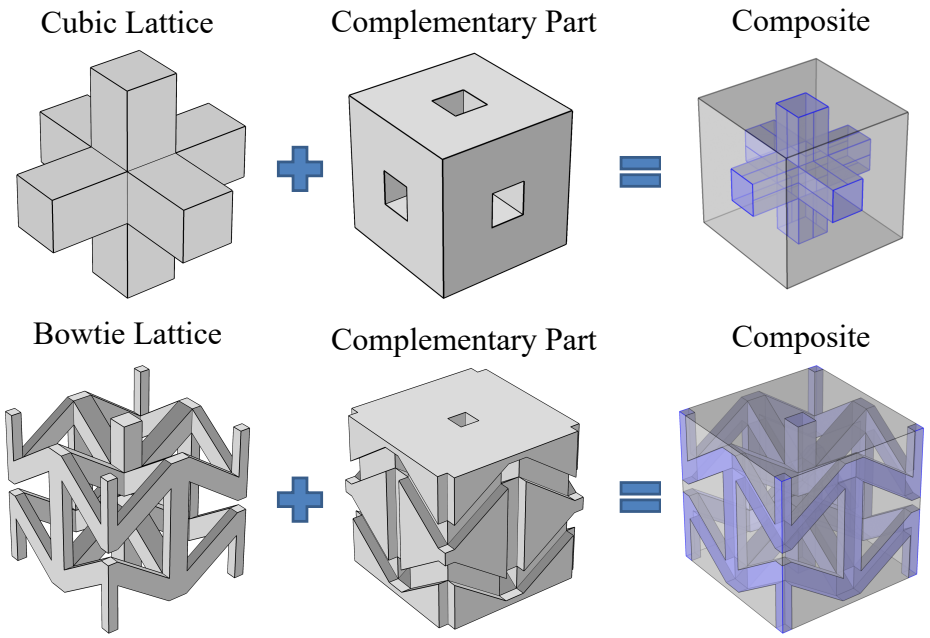

Figure 20: Composite structure solid modeling (complementary part is designed by subtracting lattice geometry from bulk unit cell volume). (Reproduced from [https://doi.org/10.1121/1.5091690], with the permission of AIP Publishing).

As a final demonstration of the Bloch-wave homogenization method, we design 3D periodic composite structures with lattice reinforcements and evaluate their effective properties. We extend Bloch-wave homogenization method to analyze periodic lattices embedded in a second solid material, referred to as 'composite structures'. We manipulate these composite structures in terms of their geometry, truss thickness, and bulk material properties to obtain variations in their elastic properties and anisotropy. We design these composite structures by filling the volume surrounding to the lattice (within the unit cell) with a second material. These composite structures enable us to obtain properties that are a mixture of two bulk materials and the lattice geometry. They are potential multifunctional metamaterials, as such structures

have already shown enhanced macroscopic strength and energy absorption properties [70]. Such composite structures can be readily fabricated by commercial multi-material 3D printers. Once the lattice geometry is modeled, we form the complementary part of this lattice within the unit cell using Boolean operations and then combine these two designs to form a composite structure (Fig. 20). We assume a complete bonded contact (no slip) between the lattice and filler material surface. This ensures the displacement continuity at the interface and satisfies mechanical compatibility during quasi-static and Bloch-wave analysis.

Here, we study composites formed from cubic, octet and bowtie lattices. We manipulate the properties and anisotropy of these composites by changing the modulus of the filler material. We keep the same lattice bulk material properties as before, and consider three cases of the filler material with moduli ratio (MR: ratio of filler bulk Young's modulus to lattice bulk Young's modulus): 50% ($E_{filler} = 0.5$ GPa), 5% ($E_{filler} = 0.05$ GPa) and 0.5% ($E_{filler} = 0.005$ GPa). To isolate the effect of modulus change, we model the density and Poisson's ratio of the filler material the same as that of the lattice bulk material.

9.1 Effective Properties of Bowtie Composite Structures

As an example, we present the effective properties of the bowtie composite, with filler moduli ratio of 0.5% (Fig. 21a) evaluated through Bloch-wave homogenization. This bowtie composite structure is auxetic up until internal cell angle, $\alpha_{aux} = 80^\circ$ (Fig. 21a) as opposed to pure bowtie lattice where $\alpha_{aux} \approx 87.5^\circ$ (Fig. 15f). For the higher moduli ratios (5% and 50%), the bowtie composite is no longer auxetic (within studied range of internal cell angles),

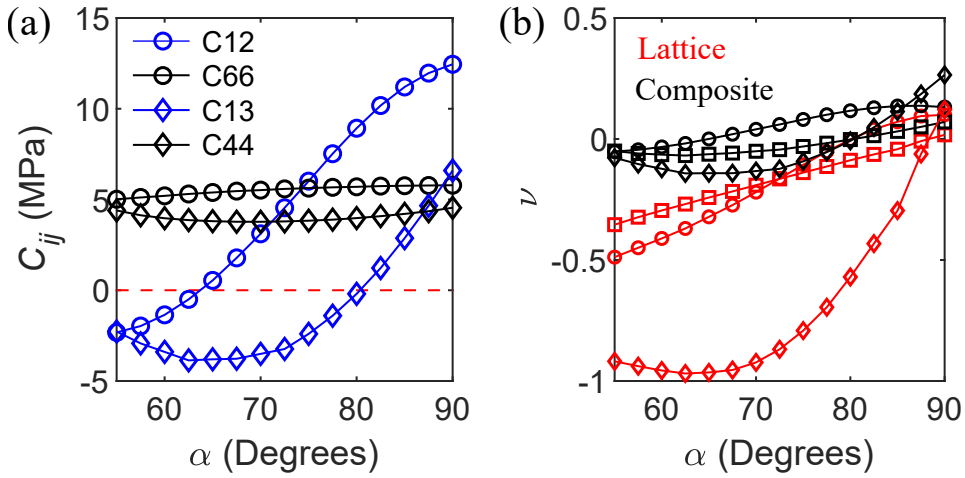

Figure 21: Effective stiffness tensor constants of the bowtie composite structure with 0.5% moduli ratio: (a) C_{12}, C_{66}, C_{13}, C_{44} (dashed red line is a zero-reference line), and (b) Poisson's ratio of bowtie lattice (red) compared to bowtie composite structure (black) (ν_{xy}, ν_{xz}, ν_{zx} are shown in circle, square and diamond markers, respectively). Reproduced from [https://doi.org/10.1121/1.5091690], with the permission of AIP Publishing)

as the filler material counteracts the deformation pattern of the re-entrant trusses (results not shown). In the case of 0.5% MR, the change in faster wave polarization is not observed even though the composite structure is auxetic, since the magnitude of the diagonal stiffness tensor constants corresponding to shear are always higher than the off-diagonal negative stiffness tensor constants (Fig. 21a). The change in the sign of Poisson's ratio is also observed at a different lattice geometry (Fig. 21b): in the XY plane, $\alpha_{aux} \approx 65°$ ($\alpha_{aux} = 80°$ in the pure lattice), whereas in the XZ plane $\alpha_{aux} \approx 80°$ ($\alpha_{aux} \approx 87.5°$ in the pure lattice). The overall stiffness of the composite structure is also higher than the pure bowtie lattice stiffness (Fig. 21a and Fig. 14f). These results show that in addition to changing the geometric parameters, changing the modulus of filler materials in composite structures can tune the overall macroscopic elastic performance of the structure.

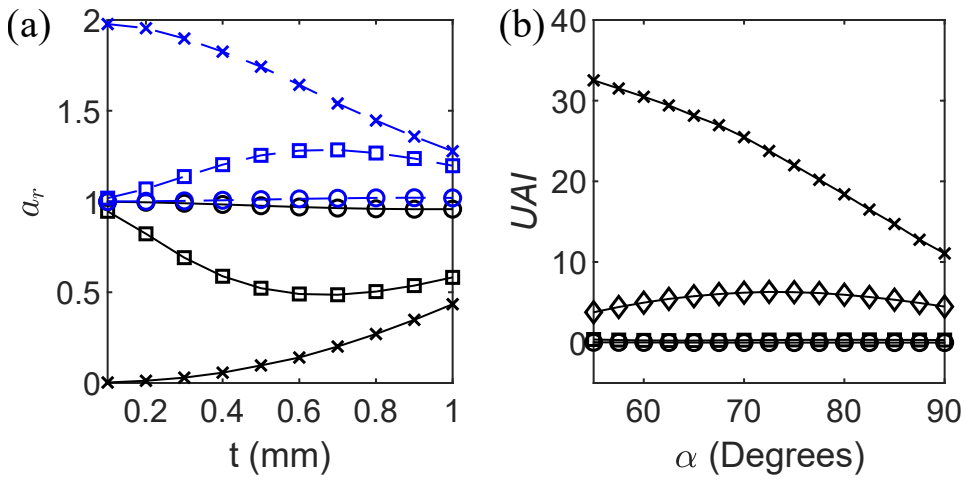

Figure 22: (a) Zener anisotropy index of cubic symmetry lattices and composites. Cubic and octet results are shown in black solid and blue dashed linestyle, respectively, and lattice, 5% and 50% MR composites are shown in cross, square and circle markers, respectively. (b) Universal anisotropy index of bowtie lattice and composites. Lattice, 0.5%, 5% and 50% MR composites are shown in cross, diamond, square and circle markers, respectively. 5% and 50% MR composites UAI values are overlapping and close to zero. (Reproduced from [`https://doi.org/10.1121/1.5091690`], with the permission of AIP Publishing)

9.2 Anisotropy Index of Composite Structures

The cubic and octet composite structures are cubic in symmetry since both lattice and filler are cubically symmetric. To observe the effect of filler material on pure lattices, we evaluate Zener anisotropy index (Fig. 22a) for moduli ratio of 5% and 50%. We observe that both cubic and octet composite structures with 50% moduli ratio are nearly isotropic, specifically at lower truss thicknesses. This is because the contribution of cubic and octet lattices in the overall structural properties is comparatively negligible. As lattice truss thickness increases, the composite structure deviates slightly from this isotropic behavior. When the moduli ratio is 5%, the lattice plays a more prominent role in the overall strength; the anisotropy of the composite structure is dominated by the lattice. The maximum anisotropy of these

composites occurs at truss thickness, t, of 0.7 mm as opposed to 0.1 mm for the pure lattices.

We compare the elastic behavior of the bowtie composites with the pure lattice based on UAI evaluated through Eq. (28). For 50% and 5% moduli ratio, the composite behaves almost isotropically (UAI = 0, Fig. 22b). Again, here the stiffness is dominated by the filler material rather than the lattice. For much softer filler material (0.5% moduli ratio), the bowtie lattice maintains some anisotropy. These results show that we can decrease the anisotropy of the composite structure by increasing the modulus of the filler material.

10 Conclusion

In this thesis, we reviewed the displacement-based elastostatic and Bloch-wave homogenization methods within a finite element method framework for effective property evaluation of 3D periodic lattices. We applied these methods to evaluate effective elastic properties of anisotropic lattices with cubic, tetragonal and transversely isotropic symmetry, including an auxetic geometry. Results obtained from Bloch-wave homogenization agree well with static homogenization results for different symmetries, relative densities, truss orientations and non-principal periodicities. We compared various lattices based on their anisotropic behavior through Zener and Universal anisotropy index. We extended this approach to analyze composite structures with lattice reinforcements, and our results show that the anisotropy and elastic performance of these structures can be manipulated without modifying the lattice geometry, but instead by modifying relative bulk material properties of the lattice and surrounding material.

The Bloch-wave homogenization approach studied in this work will open new directions to study the effect of change in geometry and bulk material properties on the static as well dynamic properties of the structure simultaneously, and can accelerate the process of analyzing periodic structures to achieve certain vibration characteristics such as band gaps, mode shapes, and energy propagation, in addition to their static effective properties. By changing the anisotropy of the structure, we show it is possible to control the wave propagation in certain direction with or without minimal change in other directions. Future work in this process will include experimental verification of evaluated effective properties of lattices. This method can be extended to develop multifunctional structural materials, where tailored vi-

bration mitigation, high impact absorption, and optimum static properties are required. The bridge between wave velocities and mechanical properties of lattice structures is also useful in nondestructive evaluation (NDE) of metamaterials through wave velocity measurements. This analysis lays the groundwork to explore NDE of lattice metamaterials in terms of quantifying mechanical property degradation through ultrasonic velocity measurements.

References

[1] R. Hill, Elastic properties of reinforced solids: Some theoretical principles, Journal of the Mechanics and Physics of Solids 11 (5) (1963) 357–372 (1963). doi:10.1016/0022-5096(63)90036-X.

[2] A. S. Dalaq, D. W. Abueidda, R. K. Abu Al-Rub, I. M. Jasiuk, Finite element prediction of effective elastic properties of interpenetrating phase composites with architectured 3D sheet reinforcements, International Journal of Solids and Structures 83 (2016) 169–182 (2016). doi:10.1016/j.ijsolstr.2016.01.011.

[3] L. J. Gibson, M. F. Ashby, Cellular Solids: Structure and Properties, 2nd Edition, Cambridge Solid State Science Series, Cambridge University Press, Cambridge, UK, 1997 (1997). doi:10.1017/CBO9781139878326.

[4] J. B. Berger, H. N. Wadley, R. M. McMeeking, Mechanical metamaterials at the theoretical limit of isotropic elastic stiffness, Nature 543 (7646) (2017) 533–537 (2017). doi:10.1038/nature21075.

[5] A. S. Phani, J. Woodhouse, N. A. Fleck, Wave propagation in two-dimensional periodic lattices, The Journal of the Acoustical Society of America 119 (4) (2006) 1995–2005 (2006). doi:10.1121/1.2179748.

[6] M. Ashby, Materials Selection in Mechanical Design Third Edition, 1992 3 (2005) 624 (2005). doi:10.1051/jp4:1993701.

[7] J. Bauer, S. Hengsbach, I. Tesari, R. Schwaiger, O. Kraft, High-strength cellular ceramic composites with 3D microarchitecture, Proceedings of the National Academy of Sciences 111 (7) (2014) 2453–2458 (2014). doi:10.1073/pnas.1315147111.

[8] N. A. Fleck, V. S. Deshpande, M. F. Ashby, Micro-architectured materials: Past, present and future, Proceedings of the Royal Society A: Mathematical, Physical and Engineering Sciences 466 (2121) (2010) 2495–2516 (2010). doi:10.1098/rspa.2010.0215.

[9] A. S. Phani, Mahmoud I. Hussein, Dynamics of Lattice Materials, 1st Edition, Wiley, New York, 2017 (2017). doi:10.1016/S0167-8922(09)70001-X.

[10] V. S. Deshpande, M. F. Ashby, N. A. Fleck, Foam topology: Bending versus stretching dominated architectures, Acta Materialia 49 (6) (2001) 1035–1040 (2001). doi:10.1016/S1359-6454(00)00379-7.

[11] S. Pellegrino, C. R. Calladine, Matrix analysis of statically and kinematically indeterminate frameworks, International Journal of Solids and Structures 22 (4) (1986) 409–428 (1986). doi:10.1016/0020-7683(86)90014-4.

[12] Lakes Roderic, Foam Structures with a Negative Poisson ' s Ratio, Science 235 (1987) 1038–1040 (1987).

[13] R. Almgren, An isotropic three-dimensional structure with Poisson's ratio =-1, Journal of Elasticity 15 (4) (1985) 427–430 (1985). doi:10.1007/BF00042531.

[14] R. Lakes, Cellular solids with tunable positive or negative thermal expansion of unbounded magnitude, Applied Physics Letters 90 (22) (2007). doi:10.1063/1.2743951.

[15] Y. Huang, X. Lu, G. Liang, Z. Xu, Pentamodal property and acoustic band gaps of pentamode metamaterials with different cross-section shapes, Physics Letters, Section A: General, Atomic and Solid State Physics 380 (13) (2016) 1334–1338 (2016). doi:10.1016/j.physleta.2016.01.041.

[16] M. Kadic, T. Bückmann, R. Schittny, M. Wegener, On anisotropic versions of three-dimensional pentamode metamaterials, New Journal of Physics 15 (2013). doi:10.1088/1367-2630/15/2/023029.

[17] S. Nemat-Nasser, A. Srivastava, Negative effective dynamic mass-density and stiffness: Micro-architecture and phononic transport in periodic composites, AIP Advances 1 (4) (2011). doi:10.1063/1.3675939.

[18] K. T. Tan, H. H. Huang, C. T. Sun, Blast-wave impact mitigation using negative effective mass density concept of elastic metamaterials, International Journal of Impact Engineering 64 (2014) 20–29 (2014). doi:10.1016/j.ijimpeng.2013.09.003.

[19] Y. Chen, L. Wang, Harnessing structural hierarchy to design stiff and lightweight phononic crystals, Extreme Mechanics Letters 9 (2016) 91–96 (2016). doi:10.1016/j.eml.2016.05.009.

[20] M. Ruzzene, F. Scarpa, F. Soranna, Wave beaming effects in two-dimensional cellular structures, Smart Materials and Structures 12 (3) (2003) 363–372 (2003). doi:10.1088/0964-1726/12/3/307.

[21] K. H. Matlack, A. Bauhofer, S. Krödel, A. Palermo, C. Daraio, Composite 3D-printed meta-structures for low frequency and broadband vibration absorption, PNAS 113 (30) (2015) 8386–8390 (2015). doi:10.1073/pnas.1600171113.

[22] C. A. Steeves, C. Mercer, E. Antinucci, M. Y. He, A. G. Evans, Experimental investigation of the thermal properties of tailored expansion lattices, International Journal of Mechanics and Materials in Design 5 (2) (2009) 195–202 (2009). doi:10.1007/s10999-009-9094-6.

[23] A. G. Evans, J. W. Hutchinson, M. F. Ashby, Multifunctionality of cellular metal systems, Progress in Materials Science 43 (1999) 171–221 (1999).

[24] I. Arretche, K. H. Matlack, On the Interrelationship Between Static and Vibration Mitigation Properties of Architected Metastructures, Frontiers in Materials 5 (November) (2018) 68 (2018). doi:10.3389/fmats.2018.00068.

[25] H. J. Rathbun, D. D. Radford, Z. Xue, M. Y. He, J. Yang, V. Deshpande, N. A. Fleck, J. W. Hutchinson, F. W. Zok, A. G. Evans, Performance of metallic honeycomb-core sandwich beams under shock loading, International Journal of Solids and Structures 43 (6) (2006) 1746–1763 (2006). doi:10.1016/j.ijsolstr.2005.06.079.

[26] T. A. Schaedler, A. J. Jacobsen, A. Torrents, A. E. Sorensen, J. Lian, J. R. Greer, L. Valdevit, W. B. Carter, Q. Ge, J. A. Jackson, S. O. Kucheyev, N. X. Fang, C. M. Spadaccini, Ultralight Metallic Microlattices, Science (New York, N.Y.) 334 (6058) (2011) 962–965 (2011). doi:10.1126/science.1211649.

[27] L. E. Murr, S. M. Gaytan, F. Medina, H. Lopez, E. Martinez, B. I. MacHado, D. H. Hernandez, L. Martinez, M. I. Lopez, R. B. Wicker, J. Bracke, Next-generation biomedical implants using additive manufacturing of complex cellular and functional mesh arrays, Philosophical Transactions of the Royal Society A: Mathematical, Physical and Engineering Sciences 368 (1917) (2010) 1999–2032 (2010). doi:10.1098/rsta.2010.0010.

[28] D. Mahmoud, M. Elbestawi, Lattice Structures and Functionally Graded Materials Applications in Additive Manufacturing of Orthopedic Implants: A Review, Journal of Manufacturing and Materials Processing 1 (2) (2017) 1–13 (2017). doi:10.3390/jmmp1020013.

[29] T. W. Tan, G. R. Douglas, T. Bond, A. S. Phani, Compliance and Longitudinal Strain of Cardiovascular Stents: Influence of Cell Geometry, Journal of Medical Devices 5 (4) (2011) 041002 (2011). doi:10.1115/1.4005226.

[30] T. Bückmann, M. Thiel, M. Kadic, R. Schittny, M. Wegener, An elasto-mechanical unfeelability cloak made of pentamode metamaterials, Nature Communications 5 (May) (2014) 1–6 (2014). doi:10.1038/ncomms5130.

[31] C. Nimmagadda, K. H. Matlack, Thermally tunable band gaps in architected metamaterial structures, Journal of Sound and Vibration 439 (2019) 29–42 (2019). doi:10.1016/j.jsv.2018.09.053.

[32] C. Pierce, V. Chen, J. Hardin, C. Willey, J. Berrigan, A. Juhl, K. H. Matlack, Viscoelastic effects on the frequency response of elastomeric metastructures, Health Monitoring of Structural and Biological Systems XIII (April) (2019) 15 (2019). doi:10.1117/12.2513912.

[33] V. S. Deshpande, N. A. Fleck, M. F. Ashby, Effective properties of the octet-truss lattice material, Journal of the Mechanics and Physics of Solids 49 (8) (2001) 1747–1769 (2001). doi:10.1016/S0022-5096(01)00010-2.

[34] D. H. Chen, Bending deformation of honeycomb consisting of regular hexagonal cells, Composite Structures 93 (2) (2011) 736–746 (2011). doi:10.1016/j.compstruct.2010.08.006.

[35] J. Hohe, W. Becker, A refined analysis of the effective elasticity tensor for general cellular sandwich cores, International Journal of Solids and Structures 38 (21) (2001) 3689–3717 (2001). doi:10.1016/S0020-7683(00)00246-8.

[36] F. Scarpa, P. Panayiotou, G. Tomlinson, Numerical and experimental uniaxial loading on in-plane auxetic honeycombs, The Journal of Strain Analysis for Engineering Design 35 (5) (2000) 383–388 (2000). doi:10.1243/0309324001514152.

[37] J. C. Wallach, L. J. Gibson, Mechanical behavior of a three-dimensional truss material, International Journal of Solids and Structures 38 (40-41) (2001) 7181–7196 (2001). doi:10.1016/S0020-7683(00)00400-5.

[38] M. S. A. Elsayed, D. Pasini, Analysis of the elastostatic specific stiffness of 2D stretching-dominated lattice materials, Mechanics of Materials 42 (7) (2010) 709–725 (2010). doi:10.1016/j.mechmat.2010.05.003.

[39] M. S. A. Elsayed, Multiscale Mechanics and Structural Design of Periodic Cellular Materials, Ph.D. dissertation, McGill University, Montreal, Canada (2010).

[40] P. Chopra, Effective Mechanical Properties of Lattice Materials, M.A.Sc. dissertation, University of British Columbia, Vancouver, Canada (2011).

[41] Y. Lai, Y. Wu, P. Sheng, Z. Q. Zhang, Hybrid elastic solids, Nature Materials 10 (8) (2011) 620–624 (2011). doi:10.1038/nmat3043.

[42] S. Krödel, T. Delpero, A. Bergamini, P. Ermanni, D. M. Kochmann, 3D auxetic microlattices with independently controllable acoustic band gaps and quasi-static elastic moduli, Advanced Engineering Materials 16 (4) (2014) 357–363 (2014). doi:10.1002/adem.201300264.

[43] M. C. Messner, M. I. Barham, M. Kumar, N. R. Barton, Wave propagation in equivalent continuums representing truss lattice materials, International Journal of Solids and Structures 73-74 (2015) 55–66 (2015). doi:10.1016/j.ijsolstr.2015.07.023.

[44] Y. H. Lee, T. Oh, The Measurement of P-, S-, and R-Wave Velocities to Evaluate the Condition of Reinforced and Prestressed Concrete Slabs, Advances in Materials Science and Engineering 2016 (2016) 1–14 (2016). doi:10.1155/2016/1548215.

[45] U. B. Halabe, G. M. Bidigalu, H. V. S. Gangarao, R. J. Ross, E. Ecmpd, E. E. Eswd, Nondestructive Evaluation of Green Wood Using Stress Wave and Transverse Vibration Techniques, Materials Evaluation 55 (9) (1995) 1013–1018 (1995). doi:10.1080/10589750802474344.

[46] H. Ogi, M. L. Dunn, K. Takashima, H. Ledbetter, Elastic properties of a unidirectional SiCf/Ti composite: Acoustic-resonance measurements and micromechanics predictions, Journal of Applied Physics 87 (6) (2000) 2769–2774 (2000). doi:10.1063/1.372254.

[47] J. D. Achenbach, Wave propagation in elastic solids, by J. D. Achenbach, North-Holland Pub. Co.; American Elsevier Pub. Co Amsterdam, New York, 1973 (1973).

[48] A. H. Nayfeh, M. J. Anderson, Wave propagation in layered anisotropic media with applications to composites, The Journal of the Acoustical Society of America 108 (2) (2000) 471–472 (2000). doi:10.1121/1.429576.

[49] Jacek J. Skrzypek, Artur W. Ganczarski, Mechanics of Anisotropic Materials, Springer, 2015 (2015). doi:10.1007/978-3-319-17160-9.

[50] M. H. Luxner, J. Stampfl, H. E. Pettermann, Numerical simulations of 3D open cell structures - influence of structural irregularities on elasto-plasticity and deformation localization, International Journal of Solids and Structures 44 (9) (2007) 2990–3003 (2007). doi:10.1016/j.ijsolstr.2006.08.039.

[51] X. Zheng, H. Lee, T. H. Weisgraber, M. Shusteff, J. DeOtte, E. B. Duoss, J. D. Kuntz, M. M. Biener, Q. Ge, J. A. Jackson, S. O. Kucheyev, N. X. Fang, C. M. Spadaccini, Ultralight, ultrastiff mechanical metamaterials, Science 344 (6190) (2014) 1373–1377 (2014). doi:10.1126/science.1252291.

[52] H. M. Kolken, A. A. Zadpoor, Auxetic mechanical metamaterials, RSC Advances 7 (9) (2017) 5111–5129 (2017). doi:10.1039/c6ra27333e.

[53] M. Jiang, I. Jasiuk, M. Ostoja-Starzewski, Apparent elastic and elastoplastic behavior of periodic composites, International Journal of Solids and Structures 39 (1) (2001) 199–212 (2001). doi:10.1016/S0020-7683(01)00145-7.

[54] Srihari Kurukuri, Homogenization of Damaged Concrete Mesostructures using Representative Volume Elements – Implementation and Application to SLang, Master, Bauhaus–University Weimar (2002). doi:10.18419/opus-3591.

[55] F. Mouhat, F. X. Coudert, Necessary and sufficient elastic stability conditions in various crystal systems, Physical Review B - Condensed Matter and Materials Physics 90 (22) (2014) 0–3 (2014). doi:10.1103/PhysRevB.90.224104.

[56] I. Berinskii, T. Aviv, Effective Elastic Properties of Some Cellular Auxetic Materials, International Congress of Theoretical and Applied Mechanics 22 (August) (2016) 21–22 (2016).

[57] F. Bloch, Über die Quantenmechanik der Elektronen in Kristallgittern, Zeitschrift für Physik A 52 (7-8) (1929) 555–600 (1929). doi:10.1007/BF01339455.

[58] C. Kittel, Introduction to Solid State Physics, 8th Edition, Wiley, New York, 2010 (2010). doi:10.1007/978-3-540-93804-0.

[59] Voichita Bucur, Acoustics of Woods, 2nd Edition, Springer Series in Wood Science, Springer-Verlag Berlin Heidelberg, Germany, 2006 (2006). doi:10.1007/978-3-662-04931-0.

[60] A. Van Pamel, G. Sha, S. I. Rokhlin, M. J. S. Lowe, Finite-element modelling of elastic wave propagation and scattering within heterogeneous media, Proceedings of the Royal Society A: Mathematical,

Physical and Engineering Science 473 (2197) (2016) 20160738 (2016). doi:10.1098/rspa.2016.0738.

[61] R. Hedayati, M. Sadighi, M. Mohammadi-Aghdam, H. Hosseini-Toudeshky, Comparison of elastic properties of open-cell metallic biomaterials with different unit cell types, Journal of Biomedical Materials Research - Part B Applied Biomaterials 106 (1) (2018) 386–398 (2018). doi:10.1002/jbm.b.33854.

[62] C. M. Zener, S. Siegel, Elasticity and anelasticity of metals, The Journal of Physical and Colloid Chemistry 53 (9) (1949) 1468–1468 (1949). doi:10.1021/j150474a017.

[63] B. C. Abell, S. Shao, L. J. Pyrak-Nolte, Measurements of elastic constants in anisotropic media, Geophysics 79 (5) (2014) D349–D362 (2014). doi:10.1190/geo2014-0023.1.

[64] K. Helbig, M. Schoenberg, Anomalous polarization of elastic waves in transversely isotropic media, The Journal of the Acoustical Society of America 81 (5) (1987) 1235–1245 (1987). doi:10.1121/1.394527.

[65] Z. Koren, I. Ravve, Slowness domain offset and traveltime approximations in layered vertical transversely isotropic media, Geophysical Prospecting 66 (6) (2018) 1070–1096 (2018). doi:10.1111/1365-2478.12626.

[66] V. Vavryčuk, Calculation of the slowness vector from the ray vector in anisotropic media, Proceedings of the Royal Society A: Mathematical, Physical and Engineering Sciences 462 (2067) (2006) 883–896 (2006). doi:10.1098/rspa.2005.1605.

[67] R. Ledbetter, H M; Kriz, Elastic- Wave Surfaces in Solids, Physica Status Solidi 475 (114) (1982) 5–10 (1982).

[68] H. J. Lee, J. R. Lee, S. H. Moon, T. J. Je, E. C. Jeon, K. Kim, Y. Y. Kim, Off-centered Double-slit Metamaterial for Elastic Wave Polarization Anomaly, Scientific Reports 7 (1) (2017) 1–13 (2017). doi:10.1038/s41598-017-15746-2.

[69] S. I. Ranganathan, M. Ostoja-Starzewski, Universal elastic anisotropy index, Physical Review Letters 101 (5) (2008) 3–6 (2008). doi:10.1103/PhysRevLett.101.055504.

[70] L. Wang, J. Lau, E. L. Thomas, M. C. Boyce, Co-continuous composite materials for stiffness, strength, and energy dissipation, Advanced Materials 23 (13) (2011) 1524–1529 (2011). doi:10.1002/adma.201003956.